Oncogene
https://doi.org/10.1038/s41388-019-0935-y

ARTICLE

The nuclear hypoxia-regulated NLUCAT1 long non-coding RNA contributes to an aggressive phenotype in lung adenocarcinoma through regulation of oxidative stress

Laura Moreno Leon[1,2] · Marine Gautier[1,2] · Richard Allan[1,2] · Marius Ilié[2,3,4] · Nicolas Nottet[1,2] · Nicolas Pons[1,2] · Agnes Paquet[1,2] · Kévin Lebrigand[1,2] · Marin Truchi[1,2] · Julien Fassy[1,2] · Virginie Magnone[1,2] · Garrett Kinnebrew[5] · Milan Radovich[5] · Meyling Hua-Chen Cheok[6] · Pascal Barbry[1,2] · Georges Vassaux[2,7] · Charles-Hugo Marquette[2,3,8] · Gilles Ponzio[1,2] · Mircea Ivan[9] · Nicolas Pottier[10] · Paul Hofman[2,3,4] · Bernard Mari[1,2] · Roger Rezzonico[2,7]

Received: 15 August 2018 / Revised: 15 May 2019 / Accepted: 7 June 2019

Abstract

Lung cancer is the leading cause of cancer death worldwide, with poor prognosis and a high rate of recurrence despite early surgical removal. Hypoxic regions within tumors represent sources of aggressiveness and resistance to therapy. Although long non-coding RNAs (lncRNAs) are increasingly recognized as major gene expression regulators, their regulation and function following hypoxic stress are still largely unexplored. Combining profiling studies on early-stage lung adenocarcinoma (LUAD) biopsies and on A549 LUAD cell lines cultured in normoxic or hypoxic conditions, we identified a subset of lncRNAs that are both correlated with the hypoxic status of tumors and regulated by hypoxia in vitro. We focused on a new transcript, NLUCAT1, which is strongly upregulated by hypoxia in vitro and correlated with hypoxic markers and poor prognosis in LUADs. Full molecular characterization showed that NLUCAT1 is a large nuclear transcript composed of six exons and mainly regulated by NF-κB and NRF2 transcription factors. CRISPR-Cas9-mediated invalidation of NLUCAT1 revealed a decrease in proliferative and invasive properties, an increase in oxidative stress and a higher sensitivity to cisplatin-induced apoptosis. Transcriptome analysis of NLUCAT1-deficient cells showed repressed genes within the antioxidant and/or cisplatin-response networks. We demonstrated that the concomitant knockdown of four of these genes products, GPX2, GLRX, ALDH3A1, and PDK4, significantly increased ROS-dependent caspase activation, thus partially mimicking the consequences of NLUCAT1 inactivation in LUAD cells. Overall, we demonstrate that NLUCAT1 contributes to an aggressive phenotype in early-stage hypoxic tumors, suggesting it may represent a new potential therapeutic target in LUADs.

Introduction

Non-small cell lung cancer (NSCLC) accounts for at least 80% of lung cancer cases, with lung adenocarcinoma (LUAD) being the most common form (~50%). Although detection and further tumor surgical resection of early-stage NSCLC has significantly improved the survival of patients, ~50% of patients with stage I NSCLC die within 5–10 years [1, 2].

Hypoxia, a condition frequently encountered in solid tumors, activates the hypoxia-inducible factor (HIF) transcription complex that orchestrates the expression of a myriad of genes, whose functions are to ensure neovascularization, glucose metabolism, cell survival, tumor spread, and resistance to most anticancer drugs [3, 4]. Not

These authors contributed equally: L. Moreno-Leon, M. Gautier

These authors contributed equally: B. Mari, R. Rezzonico

Supplementary information The online version of this article (https://doi.org/10.1038/s41388-019-0935-y) contains supplementary material, which is available to authorized users.

✉ Bernard Mari
mari@unice.fr

✉ Roger Rezzonico
rezzonico@ipmc.cnrs.fr

Extended author information available on the last page of the article

Published online: 15 August 2019

surprisingly, the HIF1A transcript is part of a prognostic classifier signature of five genes in stage I LUAD [5] and high expression of its downstream targets such as CA9 (carbonic anhydrase 9) is a predictor of worse survival [6].

Extensive evidence demonstrates that microRNAs (miRNAs) are key components of the adaptive response to low oxygen in tumors [7, 8]. We have notably underlined the central role of the prototypical "hypoxamiR" miR-210 on tumor metabolic changes and on radio-resistance in lung cancer [9, 10].

Considerable attention has recently been focused on the emerging class of long non-coding RNAs (lncRNAs), with more than 10,000 transcripts validated to date. LncRNAs, defined as transcripts longer than 200 nucleotides that do not encode proteins, are usually transcribed at lower abundance than mRNAs in a tissue-specific manner and they usually exhibit a poor primary sequence conservation [11–13]. LncRNAs encompass pseudogenes, natural antisense transcripts (NATs), and the long intervening non-coding RNAs (lincRNAs). Many lncRNAs function as part of ribonucleoprotein complexes that regulate gene expression through diverse molecular mechanisms including recruitment of transcriptional activators or repressors, chromatin epigenetic modifications, or control of mRNA processing, translation, or stability [13].

Integrative genomic analyses have identified lncRNAs with a prognostic potential that may play a role in tumor progression in four types of cancers, including lung squamous cell carcinomas (LUSCs) [14]. Moreover, several lncRNAs map to regions associated with disease by genome-wide association studies and accumulating evidence has demonstrated that they control gene networks that are relevant to cancer development and metastasis [15]. Some lncRNAs regulated by hypoxia are notably involved in metabolic adaptation and tumor spreading [16–20].

However, only a few predicted human lncRNAs among thousands have been well characterized for their expression pattern, structure, precise function, and clinical significance, especially in the context of NSCLC and of their hypoxia-mediated aggressiveness [21–23].

In this context, we performed a comprehensive genome-wide profiling to define hypoxia-regulated lncRNAs in a early-stage LUAD cohort and in a LUAD cell line in vitro. Among several "hypoxia-lncRNA" candidates, we identified NLUCAT1, a large nuclear lncRNA, which was upregulated in hypoxic conditions in LUAD cell lines and overexpressed in early-stage LUADs according to their hypoxic and overall survival (OS) status. Through CRISPR-Cas9-mediated invalidation, we demonstrated the pro-tumoral properties of NLUCAT1 and we showed that this transcript is associated with the regulation of cell proliferation, cell invasion, and cell survival in response to oxidative stress, and could, consequently, represent a new target for future therapies.

Results

Genome-wide profiling of hypoxia-regulated lncRNAs in LUAD

The identification of lncRNAs controlled by hypoxia in LUAD was performed through a combination of profiling approaches using microarrays enriched for lncRNA probes, on both clinical samples and cultured cell lines. First, we performed a transcriptomic profiling on lung samples from 57 early-stage LUAD patients (Supplementary Table S1 and Dataset 1) that were a posteriori classified in highly, moderately, and non-hypoxic groups using a metagene signature [24]. We overall found that 775 transcripts were differentially expressed between tumor and normal lung tissue, and positively correlated with the hypoxic status of tumors, whereas 1225 transcripts were negatively correlated with this hypoxic status. Among these genes, 81 potential lncRNAs were associated with the hypoxic status of the tumors (Fig. 1a and Supplementary Table S2). In parallel, we identified 78 predicted lncRNAs that are modulated in hypoxic condition in the A549 LUAD cell line (Fig. 1a, Supplementary Table S2, and Dataset 2). The comparative analysis of these data identified three lincRNAs (LINC00152, LUCAT1/Lnc-ARRDC3-1, Lnc-FAM113B-5), three pseudogenes (FER1L4, GAPDHP14, TLI1P2), and one NAT (MIF-AS1), which were upregulated by hypoxia both in vivo and in vitro, and conversely one pseudogene, PLAC9P1, which was repressed under oxygen deprivation (Fig. 1a, b).

LUCAT1/Lnc-ARRDC3-1 is a new "hypoxia-lncRNA"

We focused our attention on the LUCAT1/Lnc-ARRDC3-1, the short isoform SCAL1 of which has previously been shown to be induced by cigarette smoke extracts in NSCLC cell lines [25]. We showed that LUCAT1/Lnc-ARRDC3-1 expression is directly correlated with the hypoxic status of tumors (Fig. 1c). In addition, microarray data showed that eight out of ten probes located within this locus detected a significant increase in LUCAT1/Lnc-ARRDC3-1 expression in A549 cells cultured under hypoxic conditions (Fig. 1d). RNA sequencing (RNA-seq) analysis of A549 cells cultured under normoxic or hypoxic conditions also showed reads aligned all along the genomic region of the *LUCAT1/Lnc-ARRDC3-1* locus (chr5: 90597137-90610208) and validated induction by hypoxia (Fig. 2a). In agreement, using distinct quantitative PCR (qPCR) assays distributed throughout the locus, we confirmed the induction of

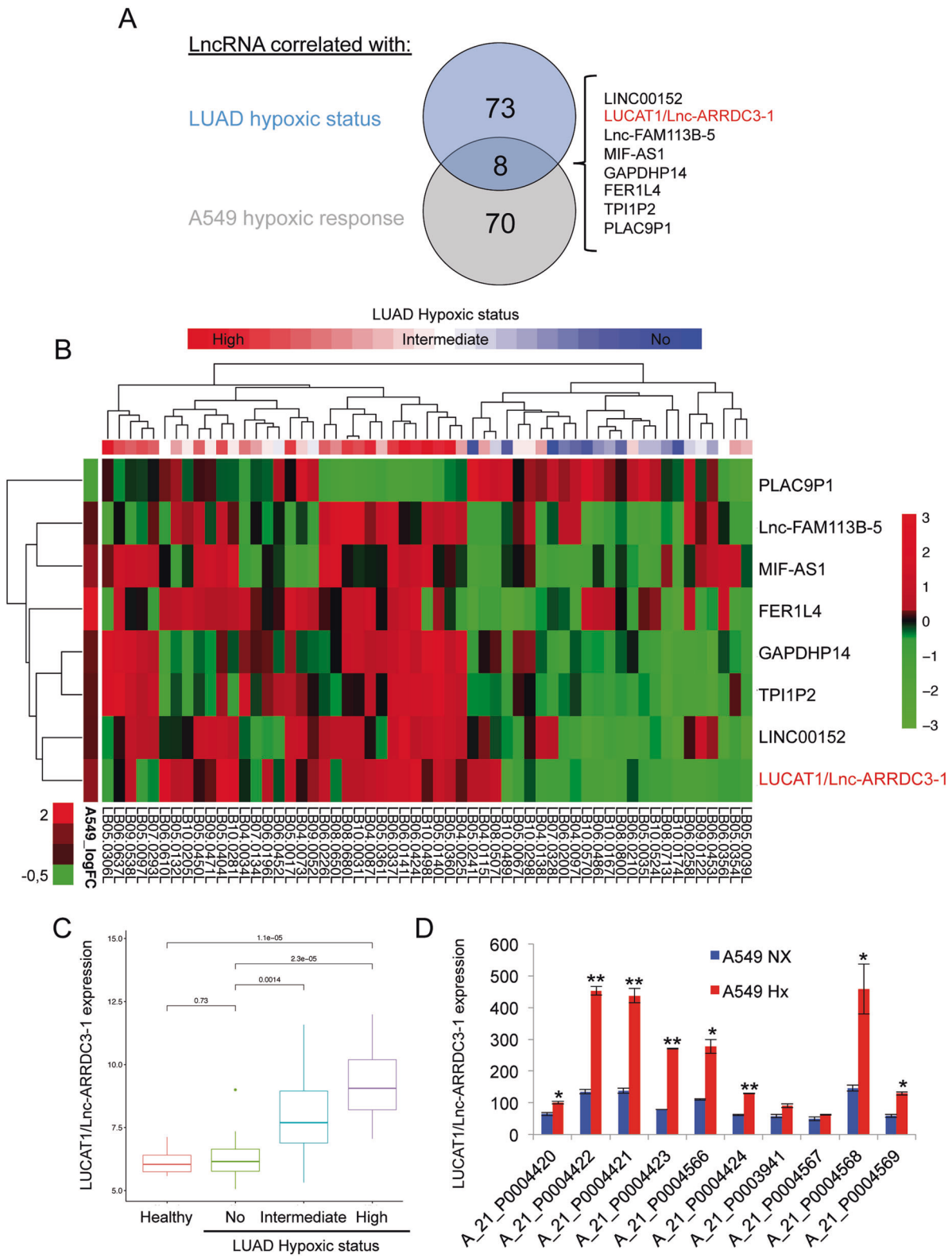

LUCAT1/Lnc-ARRDC3-1 by hypoxia in two other LUAD cell lines (Supplementary Fig. S1).

We further investigated the expression of this transcript in RNA-seq datasets from The Cancer Genome Atlas (TCGA) database (Supplementary Table S3). The analysis of 535 LUAD and 502 LUSC RNA-seq profiles confirmed that LUCAT1/Lnc-ARRDC3-1 is upregulated in relation to the hypoxic status of tumors in LUAD and, to a lesser

◀ **Fig. 1** Identification of the LUAD hypoxia-regulated LncRNA signature. **a** Venn diagram summarizing lncRNA candidates that are modulated by hypoxia in LUAD biopsies and in the A549 LUAD cell line. LncRNA expression was first analyzed by microarray hybridization in 57 early-stage LUAD and 11 peritumoral healthy lung biopsies. Tumor samples were classified by function of their hypoxic status score and selection of hypoxia-associated lncRNAs was performed using $\log_2$(intensity) > 7, absolute $\log_2$(LUAD/Healthy) > 0.7, FDR < 0.05 and adj. *P*-value hypoxic status pca < 0.05. LncRNA signature of A549 LUAD cells cultured in normoxic or hypoxic conditions for 24 h was done using $\log_2$(intensity) > 7, absolute $\log_2$(Hx/Nx) > 0.7 and adj. *P*-value < 0.05. The eight overlapping "hypoxia-lncRNA" candidates that are both deregulated by hypoxia in vivo and in vitro are shown. **b** Heatplot showing the profile of expression of the 8 "hypoxia-lncRNA" candidates in the 57 LUAD samples depending on their hypoxic status (High in red, No in blue). Expression corresponds to $\log_2$ intensity followed by median centering; clustering was performed using a Manhattan distance metric and average linkage. Differential expression between normoxic and hypoxic A549 cells is displayed as $\log_2$ fold change on the left. **c** Boxplot representation of LUCAT1/Lnc-ARRDC3-1 expression in peritumoral healthy lungs ($n = 11$) and in LUAD sample subsets according to their hypoxic status (No $n = 12$, intermediate $n = 25$, High $n = 20$). The results are displayed on a $\log_2$ scale. Statistical relevance of the comparisons was determined with the Wilcoxon's test. **d** Level of expression of LUCAT1/Lnc-ARRDC3-1 transcripts detected by the ten microarray probes spanning the LUCAT1/Lnc-ARRDC3-1 locus in A549 cells in normoxia or hypoxia. Data are means ± SD from two replicates. Statistically significant differences are indicated (*$p < 0.05$, **$p < 0.01$)

extent, in LUSC samples (Fig. 2b). This increase in expression takes place in early-stage LUAD and LUSC with no supplemental exacerbation in more advanced stages (Fig. 2c). We then evaluated the impact of LUCAT1/Lnc-ARRDC3-1 expression on patient prognosis. LUAD patients assigned to the LUCAT1/Lnc-ARRDC3-1 upper-quartile group exhibited a statistically shorter OS time than those in the lower-quartile group (log-rank test $p = 0.0012$) (Fig. 2d).

Characterization of NLUCAT1, a large nuclear variant of LUCAT1/Lnc-ARRDC3-1

Currently, only two short LUCAT1/Lnc-ARRDC3-1 transcripts of 890 nt (LUCAT1:4) and 582 nt (LUCAT1:5), respectively, are listed in the Refseq database (Fig. 2a). However, as indicated, more than 20 distinct LUCAT1 predictive transcripts ranging from 212 nt to 9585 nt are annotated in the LNCipedia database, which regroups RNA-seq information from various sources (Broad Institute, Gencode, NONCODE, Refseq, Ensembl…) [26]. Based on this complex situation and on the poor definition of the transcript boundaries frequently associated with lncRNA sequences, we performed additional characterization of the main LUCAT1/Lnc-ARRDC3-1 species transcribed from this locus. Northern blot hybridizations with probes designed in putative exons 1, 5, and 6 of LNCipedia LUCAT1/Lnc-ARRDC3-1 annotated transcripts detected a major ~ 10 kb band markedly stimulated by hypoxia and an upper 12–13 kb isoform that likely corresponds to the unspliced LUCAT1/Lnc-ARRDC3-1 pre-LncRNA (Fig. 3a). Other, less abundant transcript variants were visualized including a faint transcript at around 900 nt that matched with the LUCAT1:4 isoform. To precisely define the exon composition of the main 10 kb isoform, we combined RNA-seq and reverse transcriptase-PCR (RT-PCR) approaches (Fig. 3b, c). We concluded that this main LUCAT1 variant is a 9807 nt transcript constituted of six exons (Supplementary Information). Moreover, we demonstrated that this transcript is almost exclusively localized in the nuclei of LUAD cells, with a nucleocytoplasmic ratio similar to that of NEAT1 or MALAT1 (Fig. 4). Based on this specific attribute, we named it NLUCAT1, for nuclear-LUCAT1.

Recent reports have shown that a large proportion of lncRNAs are unstable [27, 28]. Hypoxia/reoxygenation experiments and transcription inhibition with actinomycin D demonstrated that NLUCAT1 is indeed a short-lived non-coding transcript (half-life < 1 h), suggesting that it could exert regulatory rather than housekeeping functions (Supplementary Fig. S2).

Hypoxia mainly controls gene expression through HIF, but also through activation of nuclear factor-κB (NF-κB) and/or NRF2, which are involved in hypoxia-induced inflammatory and antioxidant responses, respectively [29–31]. To better decipher NLUCAT1 regulation after hypoxic stress, we assessed the role of these transcription factors, as HRE (hypoxia response elements) and also NF-κB and NRF2 (ARE, antioxidant responsive element) consensus binding sites were found in the promoter region of the transcript. As expected, HIF1A inactivation by RNA interference (RNAi) blocked induction of the hypoxic marker CA9 but had no significant effect on NLUCAT1 expression, whereas HIF2A knockdown reduced NLUCAT1 induction by 30% (Supplementary Fig. S3A). Pharmacological inhibition of NF-κB-dependent transcription with BMS-345541 [32] totally abolished hypoxia-dependent NLUCAT1 upregulation (Fig. S3B). Accordingly, NLUCAT1 was also induced by the NF-κB-activating proinflammatory cytokine interleukin (IL)-1β in three LUAD cell lines (Supplementary Fig. S3C). As expected, this induction, along with that of the *PTGS2* inflammatory gene, was inhibited by BMS-345541 treatment. Finally, small interfering RNA (siRNA)-mediated depletion of NRF2 decreased both the basal and hypoxia-induced expression level of NLUCAT1 by 50% (Supplementary Fig. S3D). Chromatin immunoprecipitation (ChIP) coupled to qPCR was then performed to assess the direct interaction of these transcription factors with the promoter region of *NLUCAT1*. For this purpose, we used data from the ENCODE Consortium for several available human cell lines

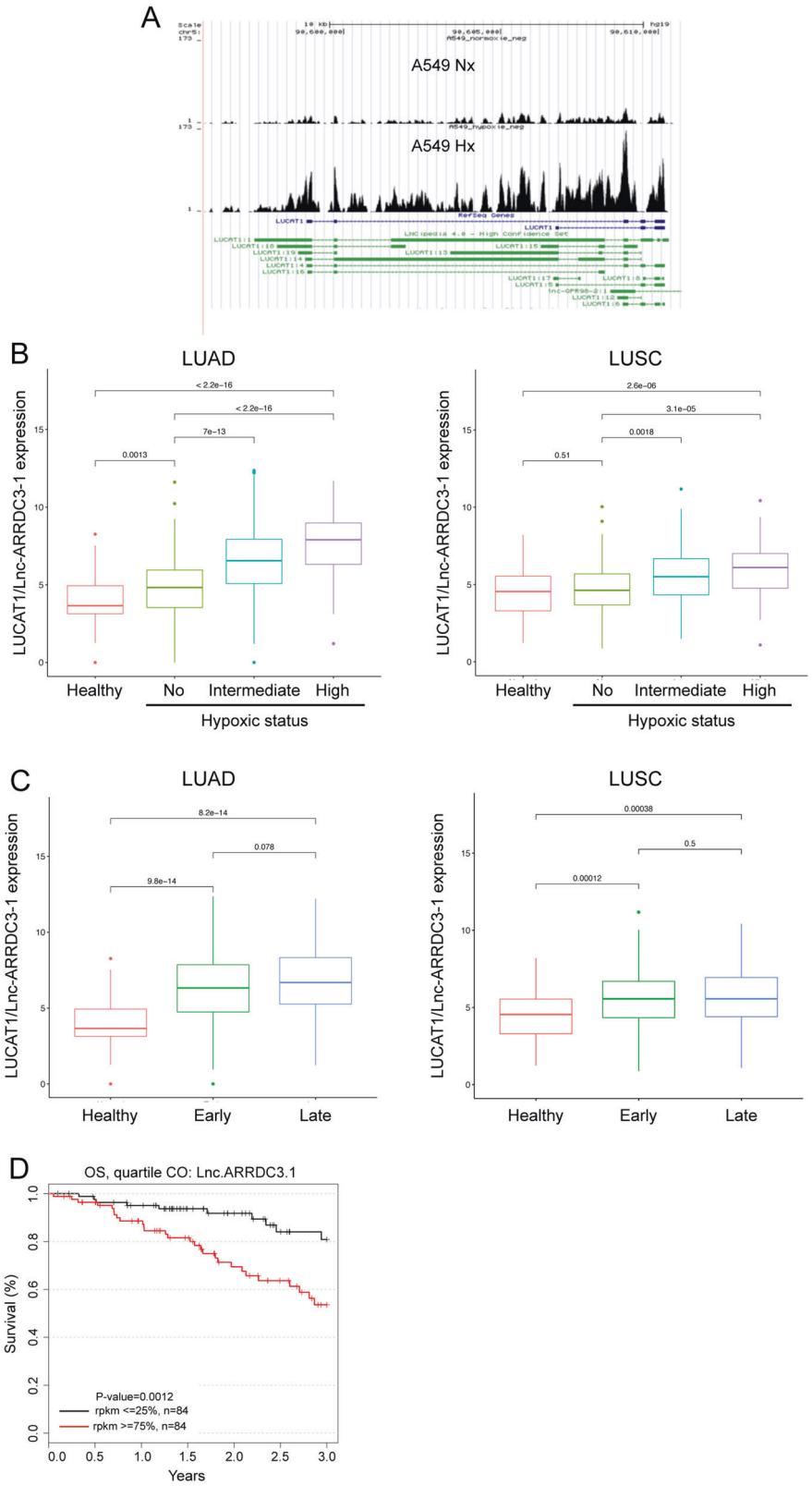

Fig. 2 LUCAT1/Lnc-ARRDC3-1 is upregulated by hypoxia in vivo and in vitro. **a** Screenshot from UCSC browser displaying *LUCAT1/Lnc-ARRDC3-1* genomic locus on chromosome 5, including the Refseq and LNCipedia database transcript annotations as well as raw RNA-seq reads plotted for A549 cells cultured for 24 h in normoxic or hypoxic conditions. **b** Distribution of LUCAT1/Lnc-ARRDC3-1 expression in LUAD and LUSC cohorts from TCGA according to their hypoxic status (LUAD: Healthy $n = 59$, No $n = 121$, Intermediate $n = 311$, High $n = 103$) (LUSC: Healthy $n = 49$, No $n = 52$, Intermediate $n = 346$, High $n = 104$). RNA-seq data were normalized as described in the Materials and Methods. The results are displayed on a $\log_2$ scale. Statistical differences between samples were analyzed with the Wilcoxon's signed-rank test. **c** Boxplots showing the distribution of LUCAT1/Lnc-ARRDC3-1 expression in LUAD and LUSC cohorts from TCGA according to tumor stage (LUAD: Healthy $n = 59$, Early $n = 403$, Late $n = 111$) (LUSC: Healthy $n = 49$, Early $n = 408$, Late $n = 92$). Statistical relevance was determined with the Wilcoxon's test. **d** Kaplan–Meier analyses of correlations between the LUCAT1/Lnc-ARRDC3-1 expression level and overall survival of TCGA LUAD patients by quartiles. *P*-values were calculated using the log-rank test

and identified several putative binding sites for these factors in the close vicinity of histone 3 lysine 27 acetylation (H3K27Ac) and H3K4 mono- and tri-methylation (H3K4Me1 and H3K4Me3) marks often found near active promoters or regulatory elements (Supplementary Fig. S4A). In A549 cells cultured under hypoxia, we found a

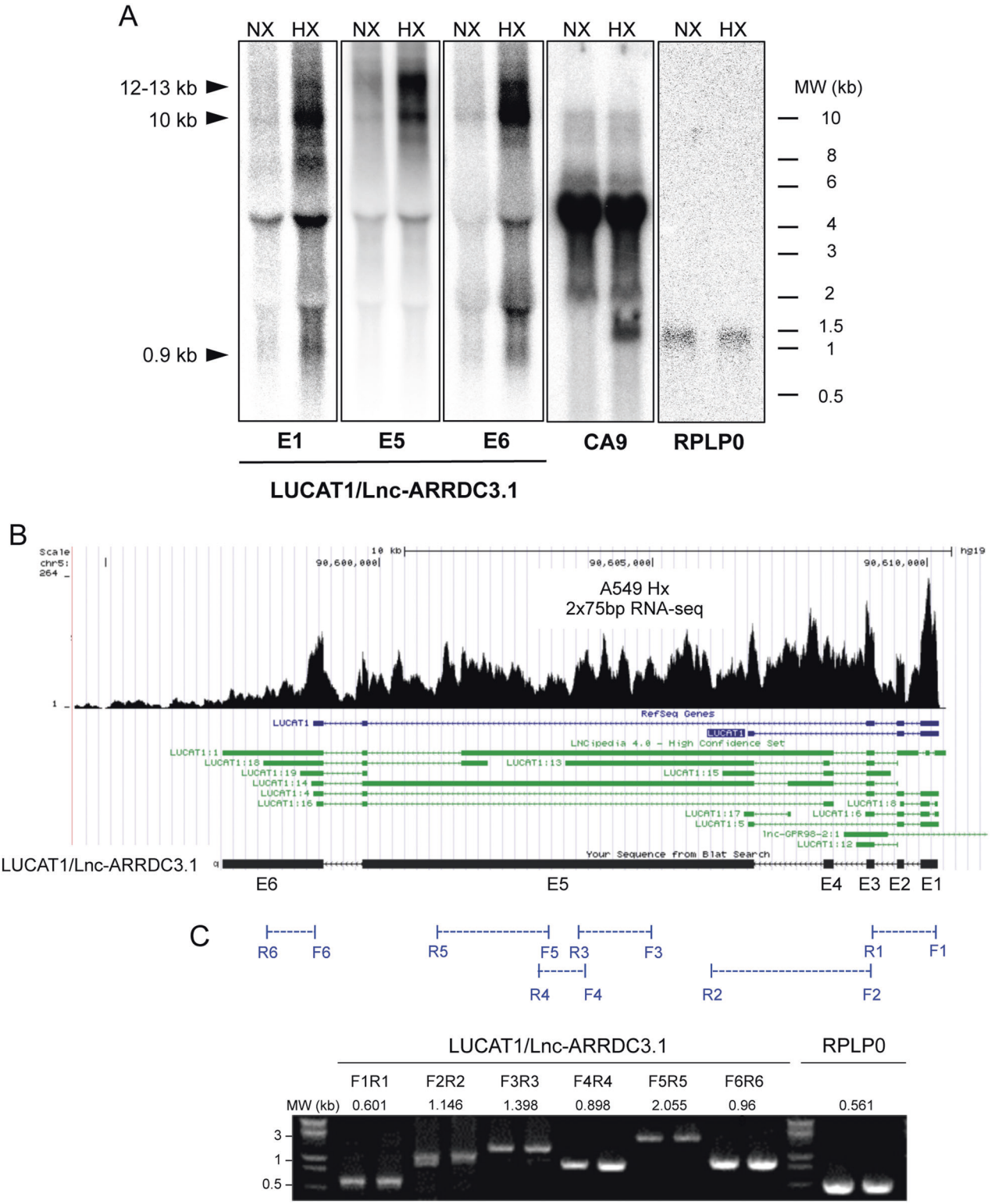

Fig. 3 Structural characterization of LUCAT1/Lnc-ARRDC3-1 transcripts in normoxic and hypoxic LUAD cell lines. **a** Northern blot analysis of LUCAT1/Lnc-ARRDC3-1 transcripts expression in A549 cells cultured for 24 h in normoxic or hypoxic conditions. Various [^{32}P]-labeled cDNA probes corresponding to putative exon 1, exon 5, and exon 6 of LNCipedia annotated LUCAT1 transcript variants were successively hybridized on blotted RNA. RPLP0 (1229 nt) and CA9 (1561 nt) hybridizations were used as loading and hypoxic response controls, respectively. **b** Screenshot from UCSC browser displaying raw RNA-seq reads for hypoxic A549 cells (NextSeq500 Illumina 75 bp paired-end reads) plotted on LUCAT1/Lnc-ARRDC3-1 genomic region and representation of de novo assembled ~ 10 kb LUCAT1/Lnc-ARRDC3-1 transcript. **c** RT-PCR analyses of LUCAT1/Lnc-ARRDC3-1 amplicons performed on two DNase-treated RNA preparations from A549 cells cultured for 24 h under hypoxia

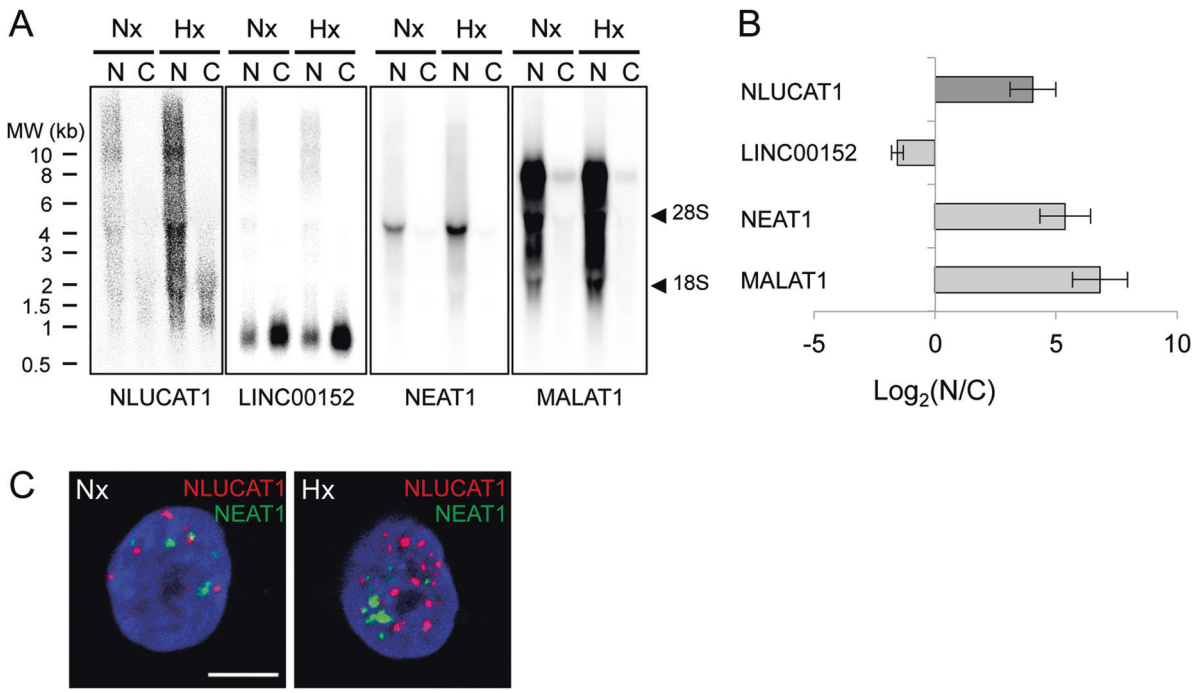

Fig. 4 NLUCAT1, a large nuclear variant of LUCAT1/Lnc-ARRDC3-1. Subcellular localization of the 10 kb LUCAT1 variant was determined on A549 cells cultured in normoxic or hypoxic conditions for 24 h using: **a** Northern blotting: total RNAs were extracted from the cytoplasmic (C) and nuclear (N) fractions, then separated, blotted, and hybridized with [^{32}P]-labeled cDNA probes for NLUCAT1 (exon 6), LINC00152, NEAT1 (short 3756 nt variant), and MALAT1. **b** qPCR: Horizontal bars represent the ratio of the expression of the indicated lncRNAs between the nucleus and the cytosol. NEAT1 and MALAT1 are specific markers of the nuclear fraction, whereas LINC00152 is exclusively cytoplasmic. Data are means ± SD from five independent experiments. **c** Single-molecule RNA-FISH (fluorescent in situ hybridization): cells were fixed and hybridized with NLUCAT1 and NEAT1 ACD® probes. Nuclei were counterstained with DAPI and cells were visualized by confocal microscopy. Scale bar corresponds to 5 µm

significant enrichment of the more distal HRE sequence (HRE3) in anti-HIF2A ChIP, as compared with control IgG (Fig. S4B). A strong binding of NRF2 was also detected in the ARE located 171 bp upstream from the transcription start site (TSS) (Supplementary Fig. S4C). Finally, we validated the interaction of three NF-κB family members, RelA, c-Rel, and p50, to the more distal NF-κB-binding site (NF-κB2) (Fig. S4D). This site was also validated for binding RelA in cells treated with IL-1β (Fig. S4E). Thus, we confirmed a direct interaction of the transcription factors HIF2A, NRF2, and NF-κB with the *NLUCAT1* promoter in LUAD cells under hypoxic environment.

Taken together, these data demonstrate that NLUCAT1 is a large, unstable, hypoxia- and inflammation-sensitive nuclear lncRNA regulated by HIF2A, NF-κB, and NRF2 transcription factors.

Targeted CRISPR-Cas9-mediated invalidation of NLUCAT1 in LUAD cells attenuates their oncogenic potential

To decipher the functional role of NLUCAT1, we developed a loss-of-function approach using CRISPR-Cas9-mediated deletion of the first three exons in the A549 cell line (Fig. 5a). After selection, individual clones were screened for the complete deletion of the three alleles (Fig. 5b), which totally abolished *NLUCAT1* transcription, as shown by RNA-seq, northern blotting, and RNA-fluorescent in situ hybridization (FISH) (Fig. 5a, c, d).

The consequences of NLUCAT1 knockout were then analyzed on distinct cellular processes using several independent clones. Cell growth was slightly but significantly (20%) decreased in NLUCAT1-deleted clones (Fig. 6a, b). We also found an increase in the basal production of reactive oxygen species (ROS) in NLUCAT1-deleted cells (Fig. 6c). Cisplatin is part of the standard first-line therapy for lung cancer and mediates DNA damage associated with mitochondrial oxidative stress [33, 34]. In this context, drug treatment produced 1.5-fold more ROS in NLUCAT1-invalidated cells than in their wild-type (WT) counterparts (Fig. 6c). Accordingly, mitochondrial superoxide production was potentiated in deleted clones in the presence of cisplatin (Supplementary Fig. S5A). Consequently, loss of NLUCAT1 expression strongly sensitized A549 cells to cisplatin-induced apoptosis visualized by caspase-3 enzymatic assay (Fig. 6d). This was reverted by an antioxidant treatment with *N*-acetyl

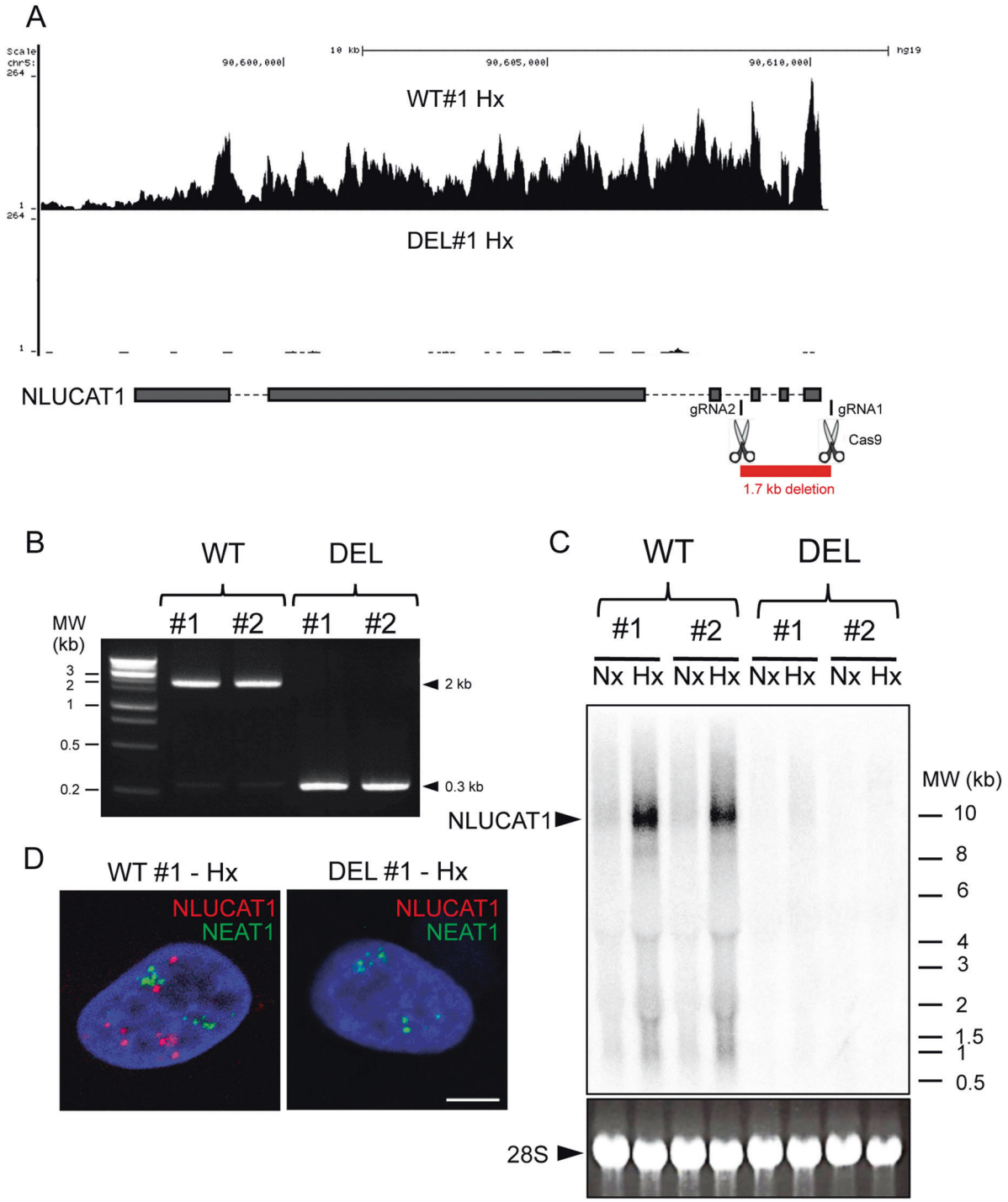

Fig. 5 CRISPR-Cas9 invalidation of the *LUCAT1/Lnc-ARRDC3-1* locus. **a** RNA-seq profile of reads mapped on the *LUCAT1/Lnc-ARRDC3-1* locus in wild-type (WT) and deleted (DEL) clones of A549 cells under hypoxia. An illustration of the strategy used for CRISPR-Cas9-mediated genomic deletion of the exon 1–3 region of the *LUCAT1/Lnc-ARRDC3-1* locus is shown (gRNA: Cas9 RNA guide). **b** PCR analysis of the 1.7 kb genomic deletion in two WT and two DEL clones of A549 cells. **c** Northern blotting analysis of NLUCAT1 10 kb transcript expression in two WT and two DEL clones of A549 cells under normoxic or hypoxic conditions using a [^{32}P]-labeled exon 6 cDNA probe. **d** Single-molecule RNA-FISH of NLUCAT1 and NEAT1 in WT and DEL clones of A549 cells under hypoxic conditions. Scale bar corresponds to 5 µm

cysteine (NAC) (Fig. 6d). Accordingly, NLUCAT1-deleted cells were more sensitive to ROS-dependent apoptosis induced by hydrogen peroxide or menadione (Supplementary Fig. S5C). In addition, NLUCAT1 invalidation slowed down the migratory and invasive properties of A549 cells (Supplementary Fig. S5B and Fig. 6e).

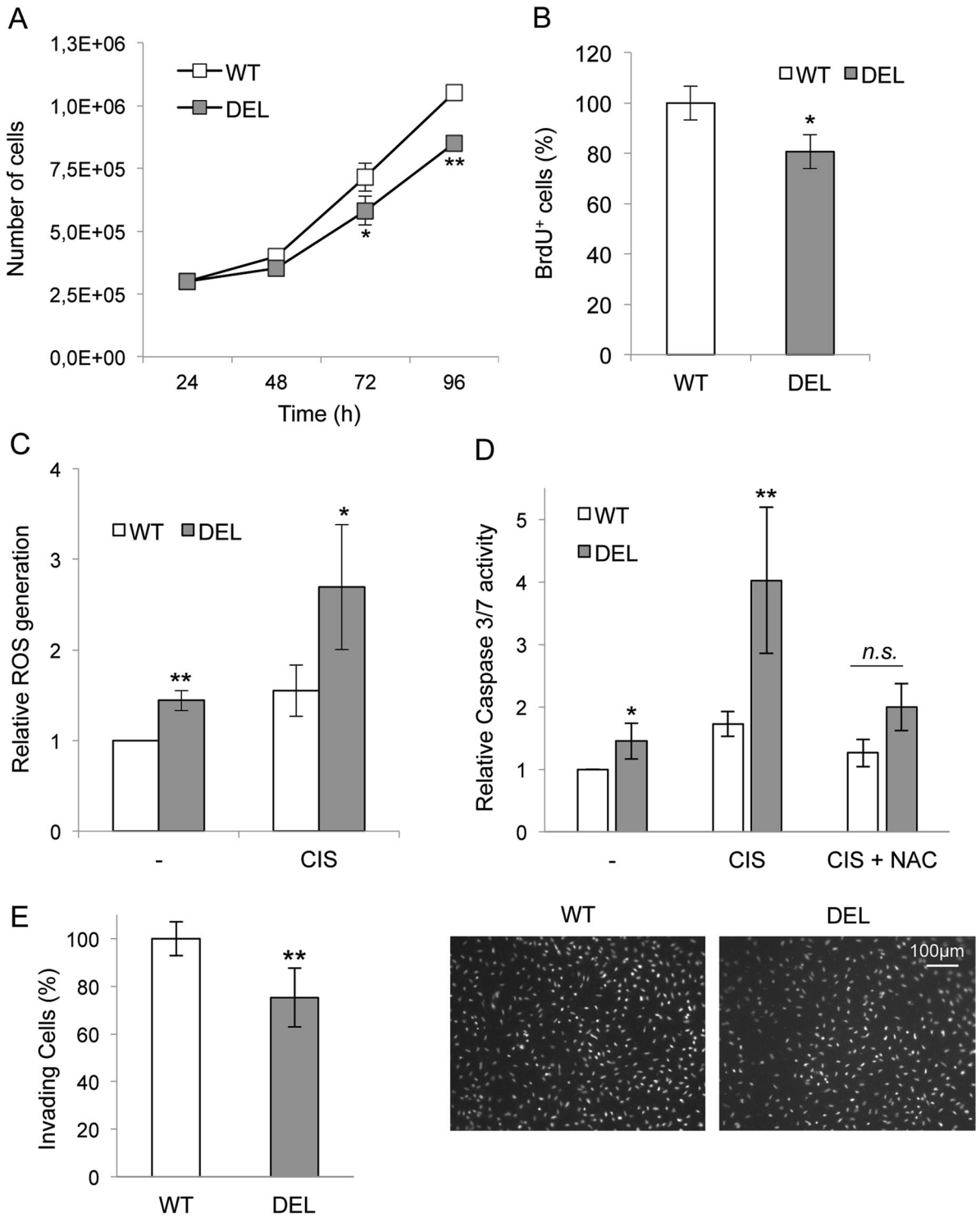

In a recent report, Thai et al. [25] suggested that the siRNA-mediated knockdown of the short LUCAT1 isoform SCAL1/LUCAT1:4 alters cell viability in the presence of cigarette smoke extract. We showed here that this minor isoform is cytosolic (Supplementary Fig. S6A) and confirmed that it is sensitive to two distinct siRNAs, whereas the major large nuclear NLUCAT1 transcript is not affected by this treatment (Supplementary Fig. S6B). Moreover, in our hands, siRNA-mediated inhibition of SCAL1/LUCAT1:4 had no impact on cell proliferation as well as on cisplatin-induced oxidative stress and apoptosis (Supplementary Fig. S6C, D, E). Furthermore, the stable re-expression of LUCAT1:4 in CRISPR-Cas9-deleted A549 clones showed no significant effect on cell proliferation,

◀ **Fig. 6** NLUCAT1 knockout affects proliferation, ROS production, cisplatin sensitivity, and invasion of LUAD cells. Effect of NLUCAT1 invalidation on: **a** cell proliferation: cells were plated (250,000/well) in triplicate and counted at the indicated times. Data are means ± SD from two individual WT and two individual CRISPR-Cas9 DEL clones of A549 cells, and are representative of three independent experiments. **b** Percentage of cells in S phase: cells were plated (250,000/well), incubated for 48 h to reach exponential growth and pulsed for 4 h with BrdU. Cells were labeled with anti-BrdU and nuclei were counterstained with DAPI. Data are expressed as percentage of BrdU-positive cells determined in four independent microscope fields. Data are means ± SD from five WT and five DEL clones of A549 cells, and are representative of three independent experiments. **c** ROS production: 48 h after plating, cells (200,000) were treated or not with 20 µM cisplatin for 24 h, then labeled with fluorescent CM-H2DCF-DA probe and analyzed by cytometry for intracellular ROS production as indicated in the Materials and Methods. Data are means ± SE from four independent experiments performed on three WT and three DEL A549 clones. **d** Caspase activity: 48 h after plating, cells (200,000) were treated or not with 20 µM cisplatin for 48 h in the presence or absence of NAC (1 mM), then lysed and analyzed for caspase-3/7 activity as indicated in the Materials and Methods. Data are means ± SE from three independent experiments performed on three WT and three DEL A549 clones. **e** Cell Invasion: cells (50,000) from WT or DEL clones were seeded in serum-free medium in the upper chambers of Matrigel-coated inserts and attracted in the lower chambers with medium containing 10% FCS and 5 ng/ml EGF. After 24 h, invading cells were scored. Data are means ± SD from two independent experiments performed on three WT and three DEL A549 clones. Statistically significant differences are indicated (*$p < 0.05$, **$p < 0.01$)

ROS production, and caspase-3 activity (Supplementary Fig. S7).

Taken together, these data clearly indicate that the major large nuclear NLUCAT1 isoform promoted an aggressive phenotype in LUAD, affecting the proliferative, cell survival, and invasive properties of tumor cells.

Impact of NLUCAT1 invalidation on the transcriptome of A549 cells

To gain further insight in the molecular mechanisms controlled by NLUCAT1, we performed transcriptomic profiling and we identified 354 genes for which the expression was significantly altered in NLUCAT1-deleted cells compared with WT clones (Fig. 7a and Supplementary Table S4). These genes were mainly (63%) repressed in NLUCAT1-deleted cells. According to our functional studies, gene annotation indicated that the modulated genes were significantly associated with Gene Ontology terms such as proliferation, invasion, apoptosis, inflammatory response, and oxidative stress (Fig. 7a, right panel).

We further validated a subset of 28 genes in independent experiments by qPCR (Supplementary Fig. S8A). Importantly, these genes were neither modulated by LUCAT1:4 RNAi in A549 cells nor by its stable re-expression in CRISPR-Cas9 *LUCAT1/Lnc-ARRDC3-1* locus-deleted clones (Supplementary Fig. S8B, C), demonstrating that the loss of short LUCAT1:4 variant expression was not involved in the gene signature alteration observed in the *NLUCAT1* locus-deleted clones.

Among the 354 genes altered by NLUCAT1 deletion, 187 were dysregulated both in normoxic and hypoxic conditions (Fig. 7b). Although the global hypoxic response appeared largely unaffected by NLUCAT1 invalidation (Fig. 7b), the transcriptome of NLUCAT1-deficient cells revealed repressed gene networks predicted to be controlled by the HIFIA, NRF2, and NF-κB transcription factors (Fig. 7c), suggesting that NLUCAT1 could exert a positive feedback on these pathways. Accordingly, concerning HIF1A, we identified 52 hypoxia-regulated genes that were altered by NLUCAT1 invalidation (Supplementary Fig. S9A). Most of these genes were upregulated under hypoxic conditions in WT cells and markedly repressed in deleted cells (Supplementary Fig. S9B, C). Among these, we notably found the well-known hypoxia-regulated gene *CA9* and the glucose transporter *GLUT3* (*SLC2A3*) (Supplementary Fig. S9C).

As NLUCAT1 knockout favored ROS production and cisplatin-induced ROS-dependent apoptosis (Fig. 6c, d and Supplementary Fig. S5A, C), we focused more specifically on NRF2, which is crucial for the maintenance of oxidative homeostasis through both hypoxia and redox signaling [31, 35]. Among the NRF2- and/or cisplatin-regulated gene networks, we identified four genes that were downregulated in NLUCAT1-knockout cells: *ALDH3A1* (aldehyde dehydrogenase 3A1), *GPX2* (glutathione peroxidase 2), *GLRX* (glutaredoxin), and *PDK4* (pyruvate dehydrogenase kinase 4) (Fig. 7d, Fig. S8A, Fig. 8a). Three of these genes products, GPX2, GLRX, and PDK4, were upregulated by hypoxia in WT cells (Fig. 8a). These enzymes either counterbalance at different levels ROS-induced damage to proteins, lipids, and DNA, or play a role in chemoresistance [36–40].

We demonstrated that the concomitant siRNA-mediated knockdown of ALDH3A1, GPX2, GLRX, and PDK4 significantly increased the production of ROS in LUAD cells (Fig. 8b), and consequently the ROS-dependent caspase-3 activation induced by cisplatin, hydrogen peroxide, or menadione, thus partially mimicking the consequences of NLUCAT1 inactivation (Fig. 8c, d).

These data indicate that the NLUCAT1-dependent regulation of these genes in LUAD cells would most likely participate in redox signaling and maintenance of oxidative homeostasis.

Discussion

Many lncRNAs are aberrantly expressed in cancer and are involved as regulators at various stages of tumorigenesis [41]. Growing evidence supports their involvement in

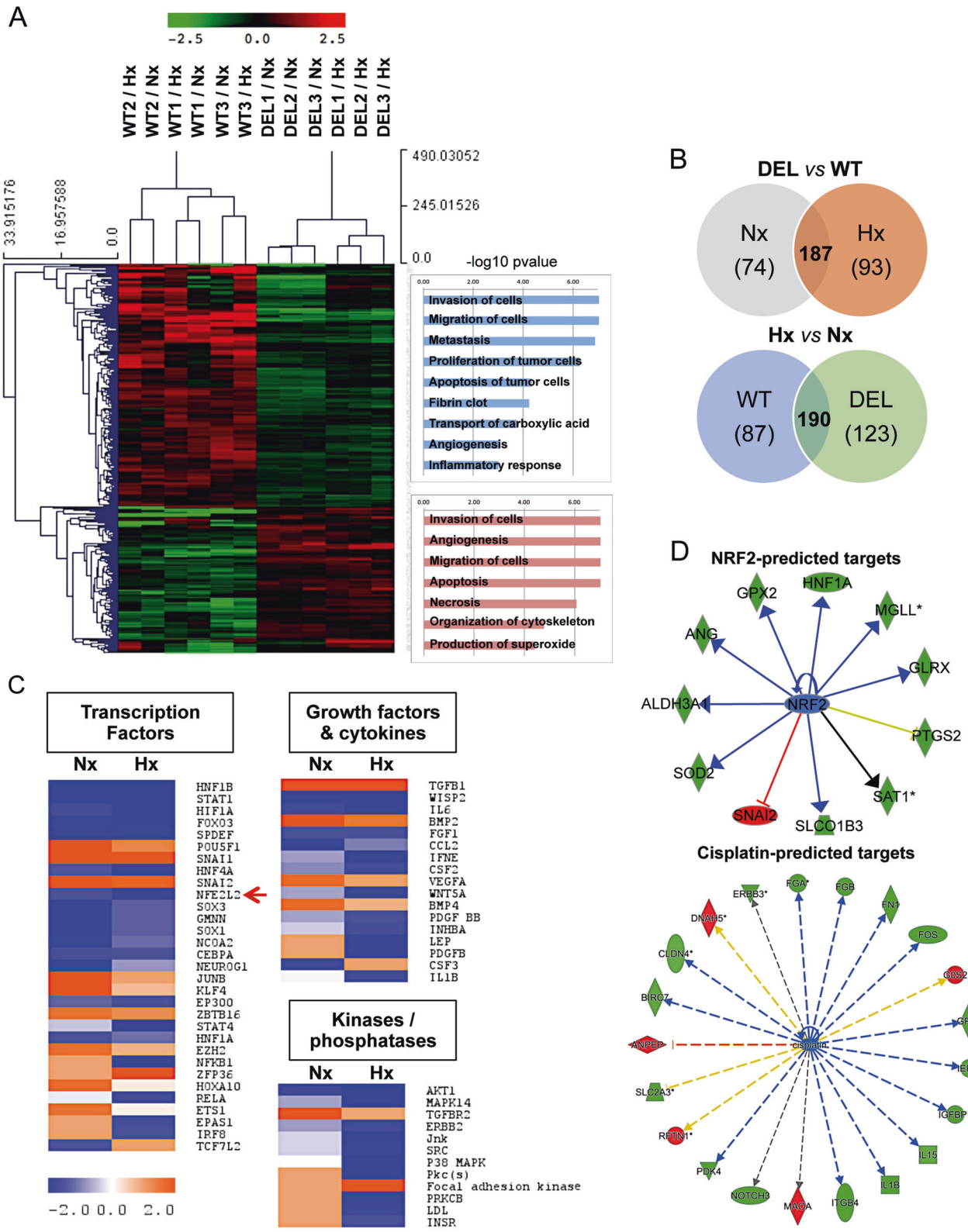

hypoxia-regulated tumor aggressiveness. Indeed, various lncRNAs, including NEAT1, H19, HOTAIR, and Linc-p21, are dysregulated in response to different cellular stresses, including hypoxia, and contribute to tumor hallmarks [20].

In the present study, we identified new "hypoxia-lncRNAs", eight of which were correlated with the hypoxic status of LUADs and also modulated by hypoxia in vitro in LUAD cell lines. We focused our attention on transcripts

◀ **Fig. 7** NLUCAT1 invalidation alters A549 cells transcriptome in normoxic and hypoxic conditions. **a** Unsupervised hierarchical clustering of differentially expressed genes between three WT and three DEL clones of A549 cells. The gene expression profiles were determined on cells cultured for 24 h in normoxic or hypoxic conditions using pan genomic microarrays. The heat map shows the 354 genes for which expression is statistically modulated by NLUCAT1 invalidation based on a $\log_2$(intensity) > 6, an absolute $\log_2$(fold change) > 1, and an adj. *P*-value < 0.01. Expression corresponds to log2 intensity followed by median centering. Clustering was performed using a Manhattan distance metric and average linkage. Gene annotation was done using the IPA software. **b** Venn diagrams comparing the distribution of genes that are (i) altered by NLUCAT1 deletion under normoxia or hypoxia ($n = 354$), or (ii) regulated by hypoxia in WT and/or DEL cells ($n = 400$, $\log_2$(intensity) > 6, an absolute $\log_2$(fold change) > 1, and an adj. *P*-value < 0.05). **c** Heatmaps of predicted upstream regulators for the comparison DEL vs. WT in normoxic or hypoxic conditions. The red arrow indicates an inhibition of NRF2-regulated transcripts. **d** Two examples of the most significant IPA NRF2- and cisplatin-regulated gene networks altered by NLUCAT1 invalidation. Genes repressed or upregulated in the signature are indicated in green and red, respectively. Orange and blue indicate activation or inhibition of the pathway, respectively

from the *LUCAT1/Lnc-ARRDC3-1* locus, because (i) the signals detected by the multiple microarray probes indicated that this was the best candidate upregulated by hypoxia in vivo and in vitro, (ii) it was validated as a "hypoxia-lncRNA" in LUAD and LUSC TCGA cohorts, and (iii) its expression was associated with lower OS.

Short-read RNA-seq profiling combined with de novo transcript-reconstruction software has provided a first draft of the lncRNA world, but this characterization remains largely incomplete [42–45]. Despite curation of cDNAs and Expressed Sequence Tags (ESTs) mainly through GENCODE annotations [46, 47], information regarding transcript structure, in particular splice junctions and boundaries, lacks precision. The LUCAT1 locus-associated transcripts represent a good example of the complexity of the lncRNA annotation situation. The LNCipedia database proposes 25 possible transcripts, annotated LUCAT1:1–1:25 [48]. Only one transcript has been functionally annotated so far and corresponds to the 890 nt lncRNA named LUCAT1:4/SCAL1 [25]. We first fully characterized the sequence, structure, and subcellular localization of the different transcript(s) produced from the *LUCAT1/Lnc-ARRDC3-1* locus.

Our data confirmed the existence of the LUCAT1:4/SCAL1 transcript in LUAD cells, but they clearly show that this represents a minor transcript product in terms of abundance, in both basal and hypoxic conditions. The major transcript corresponds to a large nuclear transcript of 9807 nt with a distinct exon structure and boundaries when compared with the 25 transcripts previously annotated so far. We thus propose the name NLUCAT1 (which may be also temporally annotated LUCAT1:26), but it appears to be critical in the future to curate most of the transcripts annotated in the different databases.

Cancer development is a complex multistep process in which hypoxic, inflammatory, and oxidative stress responses are interconnected, notably because of significant cross-talk between the HIF, NF-κB, and NRF2 transcription factors [49, 50]. Inflamed tissues frequently present highly hypoxic regions, and vice versa, which results in ROS production [51]. HIF signaling is intricately linked to that of NF-κB during hypoxic inflammation and oxidative stress activates NRF2 and NF-κB, as well as HIFs, in non-hypoxic conditions [30, 49, 52–56]. In this context, NLUCAT1 appears to be at the crossroad of these pathways, both by its transcriptional regulation and by its functional role. Indeed, we showed that in addition to being a "hypoxia-linc," NLUCAT1 is also induced by NF-κB-dependent IL-1β proinflammatory signal. Furthermore, we demonstrated that the hypoxia-dependent upregulation of NLUCAT1 is at least in part dependent on NRF2 transcription factor. These data are supported by a previous study showing that NRF2 mediates the cigarette smoke-induced expression of LUCAT1:4/SCAL1 short variant in airway epithelial cells [25]. In addition, LUCAT1:4/SCAL1 is repressed by RNAi-mediated silencing of NRF2 in A549 cells and the LUCAT1 transcripts were found to be associated with the mutation status of KEAP1 and NRF2 in LUADs and LUSCs, respectively [57, 58].

Functional annotations of gene signature alterations associated with NLUCAT1 loss-of-function revealed repressed gene networks controlled by the HIF, NRF2, and NF-κB transcription factors, suggesting that the NLUCAT1 transcript may exert a positive feedback on these pathways by a mechanism that remains to be elucidated.

Platinum-based therapy is the first-line treatment for the majority of NSCLC patients. The cytotoxic effects of cisplatin are mainly mediated by DNA-damage response but also by mitochondrial oxidative stress [33, 34]. However, resistance to these chemotherapies is frequent and increasing evidence indicates that local tumor conditions, including a hypoxic microenvironment, may be involved [59]. We showed that NLUCAT1 expression is increased in hypoxic conditions. This observation is consistent with the increased expression of LUCAT1 observed in a cisplatin-resistant human ovarian carcinoma cell line [60]. In addition, we showed that targeted deletion of NLUCAT1 decreased cell proliferation and invasion, while increasing oxidative stress-dependent sensitivity to cisplatin-induced apoptosis. By contrast, and contrary to a previously published report using an siRNA-based approach [61], we found that the short variant LUCAT1:4/SCAL1 was unable to affect these parameters. Altogether, our dataset strongly suggests that NLUCAT1 is a member of the expanding family of

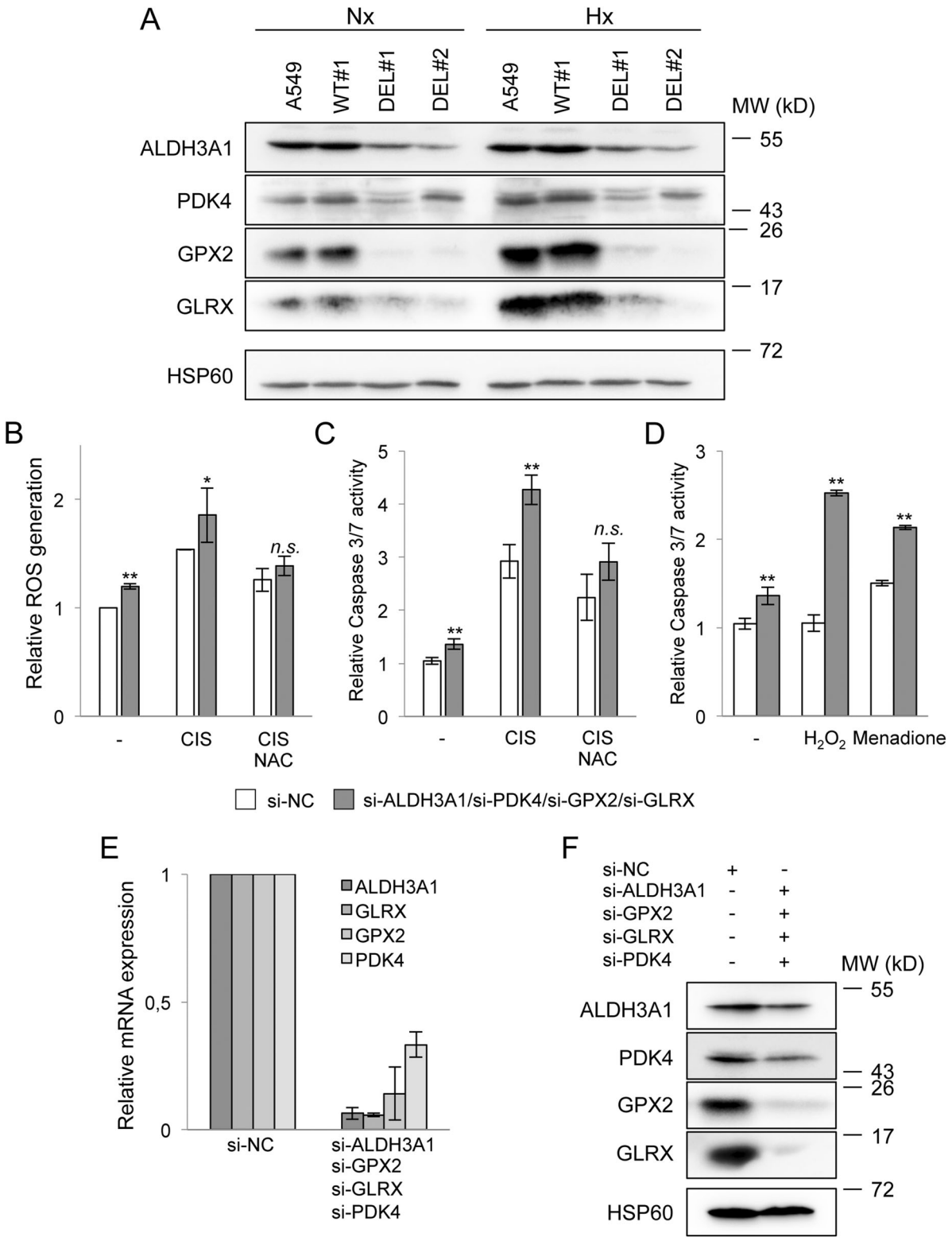

lncRNAs such as HOTAIR, UCA1, and H19 that are involved in platinum-based cancer drug resistance [62, 63].

We then focused on four genes of the NRF2- and/or cisplatin-regulated networks, all of which were downregulated in NLUCAT1-deleted cells, and which participate in drug-resistance mechanisms or redox signaling and maintenance of oxidative homeostasis to protect cells from ROS-mediated damage. In this context, GPX2

◀ **Fig. 8** Concomitant knockdown of ALDH3A1, GPX2, GLRX, and PDK4 partially mimics NLUCAT1 invalidation. **a** Western blotting analysis of ALDH3A1, GPX2, GLRX, and PDK4 expression in A549, WT, and DEL clones in normoxia or hypoxia. HSP60 was used as a loading control. **b**, **c** Effect of the concomitant RNA interference of ALDH3A1, GPX2, GLRX, and PDK4 on cisplatin-induced ROS production and caspase activity. A549 cells were plated and transfected 24 h later with 5 nM each of ALDH3A1, PDK4, GPX2, and GLRX siRNA or 20 nM non-relevant si-NC. Forty-eight hours after transfection, cells were treated or not with 20 µM cisplatin in the presence or absence of NAC (1 mM) for 24 h, after which ROS production and caspase-3/7 activity were assessed. Data are means ± SD of duplicates from two (ROS) or six (caspase) independent experiments, respectively. **d** Effect of the concomitant RNA interference of ALDH3A1, GPX2, GLRX, and PDK4 on caspase activity induced by oxidative stress: 48 h after transfection, cells were treated or not with 1 mM H_2O_2 or 100 µM menadione for 24 h, then lysed and analyzed for caspase-3/7 activity. Data are means ± SD of duplicates from three independent experiments. **e**, **f** Efficiency of concomitant RNA interference for ALDH3A1, PDK4, GPX2, and GLRX (5 nM of each) was analyzed for transcript and protein expression 48 h after transfection. Statistically significant differences are indicated (*$p < 0.05$, **$p < 0.01$)

catalyzes the reduction of hydrogen peroxide in the cytoplasm, while glutathione is oxidized to glutathione disulfide [36], thus protecting against ROS-dependent apoptosis [64, 65]. GLRX exerts its protective role against oxidative stress through the reduction of protein oxidation called deglutathionylation [37, 66]. GLRX is, notably, known to protect epithelial cells from oxidative damage via the prevention of AKT glutathionylation [37, 66]. Accordingly, GLRX downregulation could participate in the repression of an AKT-regulated pro-survival network in NLUCAT1-deleted cells (Fig. 7c). Our third candidate, ALDH3A1, neutralizes highly reactive lipid peroxidation-derived aldehydes and attenuates ROS-mediated protein modification and genotoxin-induced DNA damage and apoptosis [38, 67, 68]. Interestingly, high expression of ALDH3A1 in cancer has been associated with regulation of cell proliferation and drug resistance to ROS-dependent cyclophosphamide- and 5-fluorouracil-mediated cell death [68, 69]. Finally, PDK4, one of the four PDK family members, may favor the metabolic switch to aerobic glycolysis and chemoresistance in cancers via inhibition of the pyruvate dehydrogenase complex [39, 40]. Knockdown or inhibition of PDK4 reduced cell migration and invasion, while increasing sensitivity to 5-Fluorouracil or cisplatin in colon and/or bladder cancer cells, confirming this pro-tumorigenic function [39, 40, 70].

In agreement with these important cancer-associated functions, we demonstrated that the concomitant knockdown of these four genes in LUAD cells increased ROS-dependent apoptosis, thus partially mimicking the consequences of NLUCAT1 inactivation.

Taken together, these data suggest that dysregulation of redox signaling in NLUCAT1-deleted LUAD cells may be likely to result from an adaptation to overcome the lack of expression of NLUCAT1, which could slow proliferative and invasive properties, and sensitize cancer cells to ROS-dependent apoptosis.

Further experiments are required to fully characterize the underlying molecular mode of action of NLUCAT1 in LUAD. LUCAT1:4 short isoform has been proposed to favor cell cycle progression through epigenetic silencing of p21 and p57 cyclin-dependent kinase inhibitors due to its association with the histone methyltransferase PRC2 (polycomb repressive complex 2) [61]. This putative function is not consistent with our data, since in our hands NLUCAT1 appeared rather as a negative regulator of PRC2 signaling, as indicated in our transcriptomic analyses with a significant positive *z*-score association for EZH2 (functional enzymatic component of PRC2) in NLUCAT1-deleted cells (Fig. 7c). Moreover, although a large set of LincRNAs has been proposed to guide chromatin-modifying complexes, notably PRC2, to specific genomic loci to regulate gene expression [71], recent evidence has questioned this link, notably through the demonstration of PRC2 promiscuous RNA binding in vitro [72, 73]. Of note, the transcriptional repression induced by HOTAIR is not dependent on PRC2 as previously postulated [74]. LncRNA loci can, however, also influence the expression of neighboring genes in *cis* and some can function as enhancers, termed eRNAs, stimulating gene transcription by serving as the *cis*-regulator [75, 76]. Histone marks obtained from ChIP-sequencing assays on A549 cells of the ENCODE project indicate that NLUCAT1 is transcribed from regulatory regions enriched for H3K4me1 (mono-methylation of lysine 4 of the H3 histone protein) and H3K27ac (acetylation of lysine 27 of the H3 histone protein) marks (not shown) that are predominant histone modifications found at nucleosomes around enhancer elements. We found that CRISPR-Cas9-mediated deletion of the *NLUCAT1* TSS region slightly repressed the expression of its neighboring gene *ARRDC3* in normoxic condition but not under hypoxia. This does not support an eRNA-mediated mode of action but rather suggests that the deletion of a specific DNA regulatory element located in the vicinity of *NLUCAT1* TSS influences the basal expression of *ARRDC3*.

In summary, we provide evidence that NLUCAT1 is a new hypoxia- and inflammation-driven large nuclear lncRNA in LUAD. Targeted deletion of NLUCAT1 using a CRISPR-CAS9 strategy in the A549 cell line revealed a decrease in proliferative and invasive properties, an increase in oxidative stress, and a higher sensitivity to cisplatin-induced apoptosis, demonstrating that NLUCAT1 represents a novel coordinator of the hypoxic, inflammatory, and antioxidant responses in LUADs.

Material and methods

Cell culture and siRNA transfection

The A549, H1975, and H2228 human LUAD cell lines were obtained from ATCC (Rockville, MD). Cells were grown in Dulbecco's modified Eagle's medium (DMEM) containing 10% fetal bovine serum (Dominique Dutscher, Brumath, France). A triple gas incubator set at 1.2% oxygen, 94% nitrogen, and 5% carbon dioxide was used for hypoxic conditions. Cell lines were authenticated by PCR-single-locus technology (Eurofins, Ebersberg, Germany) and are routinely tested for mycoplasma contamination.

ON-Targetplus siRNAs (for NRF2, PDK4, GPX2, GLRX, ALDH3A1, HIF1A, HIF2A, LUCAT1:4, and negative control) were purchased from Dharmacon (Lafayette, CO). Two distinct siRNAs were used for each gene (Supplementary Table S5). Cells were plated and transfected 24 h later at 30–50% confluency, with siRNAs (5–10 nM), using Lipofectamin^{TM} RNAiMAX reagent according to the manufacturer's procedure (Thermo Fisher Scientific, Courtaboeuf, France).

Local LUAD patient cohort used for transcriptomic profiling

Fifty-seven LUAD patients hospitalized between 2004 and 2010 at the Pasteur Hospital (Departments of Pulmonary Medicine and Thoracic Surgery, CHU de Nice, France) were enrolled in this study. The diagnosis of LUAD was based on examination of all tumor specimens using the seventh pTNM classification and on the last histological classification of NSCLC. Written informed consent was obtained from participants after explaining the nature of the study, which was approved by the research ethics board of the Nice University hospital and was performed according to the guidelines of the Declaration of Helsinki. The main clinical and pathological data are summarized in Supplementary Table S1. Eleven normal lung tissue specimens were taken from areas at standard distance (3 cm) from the same cohort of patients.

Microarray hybridization and statistical analyses

Transcriptomic analyses of LUAD samples and A549 cells were performed on SurePrint G3 Human Gene Expression v2 8 × 60 K microarrays from Agilent Technology (Loveland, CO, USA) as previously described [77].

Data analyses were performed using R. We used the Bioconductor package array QualityMetrics and custom R scripts for quality control. Additional analyses were done using Bioconductor package Limma. Data were normalized using the quantile method. A linear modeling approach was used to calculate log ratios, moderated *t*-statistics, and *P*-values for each comparison of interest. *P*-values were adjusted for multiple testing using the Benjamini–Hochberg method that controls the false discovery rate.

First, we isolated lncRNAs that are differentially expressed between 57 LUAD samples and 11 peritumoral healthy lung tissues (Dataset 1). LUAD hypoxic status was determined a posteriori based on a selection of 27 genes extracted from a hypoxia-derived metagene signature [24] using a score corresponding to the number of genes with a fold change > 2 compared with the mean average expression in healthy tissues (from 0 to 27: 0–9: "no"; 10–18: "intermediate"; 19–27: "high" hypoxic). A principal component analysis strategy using this hypoxic score was then performed to calculate the correlation between hypoxia and the log-transformed gene expression values of each probe, as previously described [78]. Spearman's rank correlation was applied and probes were ranked according to *p*-values.

Two biological replicates were performed for comparison of A549 cells cultured in normoxic and hypoxic conditions (Dataset 2).

For NLUCAT1 WT and -deleted A549 clones, three distinct clones of each phenotype cultured in normoxic or hypoxic conditions were compared (Dataset 5). Enrichment in biological themes (Molecular function, Upstream regulators, and canonical pathways) and biological networks analysis were performed using Ingenuity Pathway Analysis software (http://www.ingenuity.com/). Hierarchical clusterings were performed with the MultiExperiment Viewer (MeV) program version 4.9, using a Manhattan distance metric and average linkage.

TCGA dataset analyses

We used LUAD and LUSC datasets from TCGA. RNA-seq and survival data were available for 522 and 504 patients, respectively (Supplementary Table S3). RNA-seq data were normalized using the Bioconductor package DESeq2. The hypoxic status for each sample was determined using the same method as for the local cohort. Patients were separated into high-, intermediate-, and no hypoxic status groups. Survival curves were generated using the Kaplan–Meier method and significance was assessed using the log-rank test.

RNA extraction and gene expression analyses by qPCR, RT-PCR, and northern blotting

Total RNAs were isolated with TRIzol® reagent (Thermo Fisher Scientific) or RNAeasy kit (Qiagen, Hilden, Germany) according to the manufacturer's instructions. Gene expression was measured by qPCR as previously described [79] (Supplementary Table S6). For standard

RT-PCR, genes were amplified by GoTaq DNA polymerase (Promega, Madison, WI, USA) using 100 ng cDNA and analyzed on agarose gels. All primer sequences corresponding to the different genes analyzed are in Supplementary Table S7. Northern blotting were done with 20 µg of total RNAs and quantified on a Fujifilm FLA-5100 phosphorimager.

Subcellular fractionation

Cytosolic and nuclear fractions were prepared as previously described [80], and cytosolic and nuclear RNAs were extracted with TRIzol® and TRIzol®LS reagents (Thermo Fisher Scientific), respectively.

Single-molecule RNA fluorescence in situ hybridization

LncRNA-FISH was performed using RNAscope Multiplex Fluorescent assays (Advanced Cell Diagnostics, Hayward, CA) according to the manufacturer's protocol. Two distinct sets of short oligonucleotide probes were designed for NLUCAT1: (i) a specific NLUCAT1 probe-set targeting the 3575–5860 sequence in the exon 5, and (ii) a probe-set targeting the full-length NLUCAT1 sequence (9807 bp) that detects NLUCAT1 and also the short LUCAT1:4 variant. Commercially available human *NEAT*1 and bacterial dapB probe sets were used as positive and negative controls, respectively.

Chromatin immunoprecipitation

ChIP was performed using the iDeal ChIP-qPCR kit from Diagenode (Belgium) according to the manufacturer's protocol. Briefly, cells were exposed to hypoxia (1% O_2) or IL-1β (20 ng/ml) and then cross-linked with ChIP cross-link Gold reagent (Diagenode) for 30 min and 1% formaldehyde for 15 min. Cross-linking was stopped with 0.125 M glycine. Cells were collected by scrapping, lysed at 4 °C, and resuspended in shearing buffer iS1b containing protease inhibitor cocktail. After sonication using the Bioruptor (Diagenode) to yield DNA fragments of 200–1000 bp, lysates were cleared by centrifugation at $16{,}000 \times g$ for 10 min. For each immunoprecipitation assay, lysates corresponding to 4×10^6 cells were incubated with 5 µg of rabbit antibodies pre-adsorbed on Diamag protein A-coated magnetic beads and incubated overnight at 4 °C with rotation.

After washing and proteinase digestion, the immunoprecipitates were de-cross-linked 15 min at 100 °C and genomic DNA was purified. The primers used for the amplification of the *NLUCAT1* promoter are listed in Supplementary Table S8.

CRISPR-Cas9-mediated invalidation of NLUCAT1

The sequence targeted for CRISPR-Cas9 genome modification was identified using the online design tool (http://crispr.mit.edu/). Two single-guide RNAs (sgRNAs) were selected: gRNA1, located 172 bp upstream of the TSS of *NLUCAT1*, and gRNA2, located in intron 3, 1518 bp downstream of the TSS. Sense and antisense oligonucleotides were synthesized containing the gRNA sequence, an additional 5′-end guanine nucleotide and the *BbsI* overhangs (Supplementary Table S9). The annealed sgRNAs were ligated into the *BbsI*-digested pSpCas9(BB)-2A-Puro (pX459) V2.0 plasmid (Adgene, Cambridge, MA). Inserts were sequenced for final validation.

A549 cells (1.8×10^6) were reverse transfected with 7.5 µg each of pX459-gRNA1 and pX459-gRNA2 constructs using Lipofectamine LTX® reagent (Thermo Fisher Scientific), according to the manufacturers' procedures. Selection with puromycin (2 µg/ml) was performed 24 h after transfection for at least 48 h. Cells were then cloned by serial dilution and amplified individual clones were screened for complete tri-allelic deletion on 50 ng genomic DNA using three qPCR assays (Supplementary Table S10).

RNA sequencing

Solid protocol (Dataset 3)

Two micrograms of total RNAs from normoxic or hypoxic A549 cells were depleted from ribosomal RNA with the Ribo-Zero™ rRNA removal kit (Epicentre, Madison, WI) and libraries were processed following the NEBNext® mRNA Library Prep Set for SOLiD™ (New England Biolabs, Ipswich, MA), then amplified, quantified with the Bioanalyzer High Sensitivity DNA Kit (Agilent), and sequenced on SOLiD 5500XL (Thermo Fisher Scientific) with single-end 50 bp reads. Reads were aligned to the human genome release hg19 with the LifeScope software v2.5.1 (Thermo Fisher Scientific) using whole transcriptome pipeline for RNA-seq libraries with default parameters.

Illumina protocol (Dataset 4)

Libraries were generated from 500 ng of total RNA from WT and CRISPR-Cas9-deleted A549 clones in hypoxic conditions using the TruSeq Stranded Total RNA Library Prep kit (Illumina, San Diego, CA) according to the manufacturer's instructions. Libraries were then quantified with a KAPA library quantification kit (Roche, Basel, Switzerland) and pooled. Four nanomoles of this pool were loaded onto a high-output flowcell and sequenced on a NextSeq500 sequencer (Illumina) with 2×75 bp paired-end

chemistry. Reads were aligned to the human genome release hg19 using STAR v2.4.0a with default parameters.

Cloning procedures and stable lentiviral transduction

The short 890 nt LUCAT1:4 variant (NR_103548) was synthesized as a gBlock® double-stranded DNA fragment (Integrated DNA Technologies, Leuven, Belgium) and ligated into the pLJM1 vector (Addgene) between AgeI and EcoRI sites.

Lentiviral particles were produced in 293TN cells using the pPACKH1 HIV Lentivector Packaging Kit (System Biosciences, Palo Alto, CA) with Lipofectamine LTX Plus reagent according to manufacturers' procedures. The lentiviral particles were then collected, mixed with PEG-it virus precipitation kit (System Biosciences), and concentrated 100-fold. Titration of lentiviral particles was performed on HELA cells using the Global UltraRapid™ Lentiviral Titer Kit (System Biosciences).

A549 cells (8×10^5) were transduced with pLJM1-LUCAT1:4 lentiviral particles (multiplicity of infection 5) in DMEM containing 8 µg/ml polybrene. Cells were kept under puromycin selection (2 µg/ml) 48 h after transduction until only transduced cells remained.

ROS and superoxide production

ROS and superoxide were measured by flow cytometry with the cell permeant 2',7'-dichlorodihydrofluorescein diacetate (CM-H2DCF-DA) and mitoSOX™ red fluorescent probes, respectively (Thermo Fisher Scientific). Cells were incubated in the dark with 5 µM CM-H2DCF-DA or mitoSOX™ red in Hank's buffered salt solution for 45 min at 37 °C, trypsinized, washed twice, and detection of oxidized highly fluorescent 2',7'-dichlorofluorescein or mitoSOX™ red was performed on a flow cytometer (LSR II Fortessa, BD Biosciences) using excitation wavelengths of 488 nm and 510 nm, respectively (emission 525 nm and 580 nm, respectively).

Caspase assays

The activation of executioner caspase-3 in A549 cells was determined with the Caspase-Glo 3/7 Assay kit (Promega) according to the manufacturer's instructions. Cells were lysed in passive lysis buffer and the protein concentration determined using the Pierce™ BCA Protein Assay kit (Thermo Fisher Scientific). Cell lysates (5 µg of proteins) were incubated with the caspase substrates and luminescence was quantified after 30 min and normalized to the amount of proteins.

Migration and invasion assays

Boyden's chamber assays were performed as described previously [81]. Invasion was assessed using a commercially available 24-well BioCoat Matrigel Invasion Chamber (BD Biosciences).

Statistical analyses

All experimental samples were included in the final analyses. Unless indicated otherwise, all data were representative of at least two independent experiments and expressed as means ± SD. Before statistical analysis, data were checked for normal distribution (Shapiro–Wilk's test) and comparable variance (F-test for equality of variances for data with normal distribution). Comparisons between two groups of normally distributed data with equal variances were performed using the unpaired two-sided Student's *t*-test. Differences were considered statistically significant at $p < 0.05$. Sample size (n), statistical tests, and p-values are indicated in the figure legends.

Antibodies

For ChIP experiments, rabbit anti-HIF-2α (ab199) was from Abcam (Cambridge, UK), normal rabbit IgG and rabbit anti-NRF2 (D179C-XP) were from Cell Signaling Technology (Danvers, MA, USA), and rabbit polyclonal antibodies to RelA (sc-372), NF-κB p50 (sc7178x), and c-Rel (sc-71 ×) were from Santa Cruz Biotechnology (Heidelberg, Germany). For western blotting analyses, goat polyclonal antibody to Hsp60 (sc-1052) and mouse monoclonal antibodies to GLRX (sc-293250) and ALDH3A1 (sc-376089) were purchased from Santa Cruz Biotechnology. Anti-PDK4 (AP7041B) was from Abgent (San Diego, CA, USA) and anti-GPX2 (GTX100292) from GeneTex (Irvine, CA, USA). Secondary horseradish peroxidase-conjugated antibodies were from Dako (Copenhagen, Denmark).

Data availability

The experimental data from microarray and RNA sequencing have been deposited in the NCBI Gene Expression Omnibus (GEO) database under SuperSerie GSE117049 containing 5 distinct datasets.

Acknowledgements We gratefully acknowledge the outstanding technical support of the UCA GenomiX platform and MICA imaging facility of the University Côte d'Azur, and the staff from the CHU Nice Biobank. This work was supported by Plan Cancer 2018 « ARN non-codants en cancérologie: du fondamental au translationnel » (number 18CN045), Cancéropole PACA, Fondation ARC pour la Recherche sur le Cancer, Fondation Unice (AIR project), Ligue contre le cancer (comité départemental du Nord), and the French Government

(Agence Nationale de Recherche, ANR) through the Investments for the Future LABEX SIGNALIFE (ANR-11-LABX-0028-01) and FRANCE GENOMIQUE (ANR-10-INBS-09-03 and ANR-10-INBS-09-02). LML was a recipient of the Fondation pour la Recherche Médicale.

Compliance with ethical standards

Conflict of interest The authors declare that they have no conflict of interest.

Publisher's note: Springer Nature remains neutral with regard to jurisdictional claims in published maps and institutional affiliations.

References

1. Chang MY, Mentzer SJ, Colson YL, Linden PA, Jaklitsch MT, Lipsitz SR, et al. Factors predicting poor survival after resection of stage IA non-small cell lung cancer. J Thorac Cardiovasc Surg. 2007;134:850–6.
2. Ou SH, Zell JA, Ziogas A, Anton-Culver H. Prognostic factors for survival of stage I nonsmall cell lung cancer patients: a population-based analysis of 19,702 stage I patients in the California Cancer Registry from 1989 to 2003. Cancer. 2007;110:1532–41.
3. Pouyssegur J, Dayan F, Mazure NM. Hypoxia signalling in cancer and approaches to enforce tumour regression. Nature. 2006;441:437–43.
4. Holohan C, Van Schaeybroeck S, Longley DB, Johnston PG. Cancer drug resistance: an evolving paradigm. Nat Rev Cancer. 2013;13:714–26.
5. Akagi I, Okayama H, Schetter AJ, Robles AI, Kohno T, Bowman ED, et al. Combination of protein coding and non-coding gene expression as a robust prognostic classifier in stage I lung adenocarcinoma. Cancer Res. 2013;73:3821–32.
6. Ilie M, Mazure NM, Hofman V, Ammadi RE, Ortholan C, Bonnetaud C, et al. High levels of carbonic anhydrase IX in tumour tissue and plasma are biomarkers of poor prognostic in patients with non-small cell lung cancer. Br J Cancer. 2010;102:1627–35.
7. Gee HE, Ivan C, Calin GA, Ivan M. HypoxamiRs and cancer: from biology to targeted therapy. Antioxid Redox Signal. 2014;21:1220–38.
8. Bertero T, Rezzonico R, Pottier N, Mari B. Impact of microRNAs in the cellular response to hypoxia. Int Rev Cell Mol Biol. 2017;333:91–158.
9. Puissegur MP, Mazure NM, Bertero T, Pradelli L, Grosso S, Robbe-Sermesant K, et al. miR-210 is overexpressed in late stages of lung cancer and mediates mitochondrial alterations associated with modulation of HIF-1 activity. Cell Death Differ. 2011;18:465–78.
10. Grosso S, Doyen J, Parks SK, Bertero T, Paye A, Cardinaud B, et al. MiR-210 promotes a hypoxic phenotype and increases radioresistance in human lung cancer cell lines. Cell Death Dis. 2013;4:e544.
11. Guttman M, Rinn JL. Modular regulatory principles of large non-coding RNAs. Nature. 2012;482:339–46.
12. Ulitsky I, Bartel DP. lincRNAs: genomics, evolution, and mechanisms. Cell. 2013;154:26–46.
13. Quinn JJ, Chang HY. Unique features of long non-coding RNA biogenesis and function. Nat Rev Genet. 2016;17:47–62.
14. Du Z, Fei T, Verhaak RG, Su Z, Zhang Y, Brown M, et al. Integrative genomic analyses reveal clinically relevant long non-coding RNAs in human cancer. Nat Struct Mol Biol. 2013;20:908–13.
15. Schmitt AM, Chang HY. Long noncoding RNAs in cancer pathways. Cancer Cell. 2016;29:452–63.
16. Yang F, Huo XS, Yuan SX, Zhang L, Zhou WP, Wang F, et al. Repression of the long noncoding RNA-LET by histone deacetylase 3 contributes to hypoxia-mediated metastasis. Mol Cell. 2013;49:1083–96.
17. Ferdin J, Nishida N, Wu X, Nicoloso MS, Shah MY, Devlin C, et al. HINCUTs in cancer: hypoxia-induced noncoding ultraconserved transcripts. Cell Death Differ. 2013;20:1675–87.
18. Yang F, Zhang H, Mei Y, Wu M. Reciprocal regulation of HIF-1alpha and lincRNA-p21 modulates the Warburg effect. Mol Cell. 2014;53:88–100.
19. Lin A, Li C, Xing Z, Hu Q, Liang K, Han L, et al. The LINK-A lncRNA activates normoxic HIF1alpha signalling in triple-negative breast cancer. Nat Cell Biol. 2016;18:213–24.
20. Chang YN, Zhang K, Hu ZM, Qi HX, Shi ZM, Han XH, et al. Hypoxia-regulated lncRNAs in cancer. Gene. 2016;575:1–8.
21. Schmidt LH, Spieker T, Koschmieder S, Schaffers S, Humberg J, Jungen D, et al. The long noncoding MALAT-1 RNA indicates a poor prognosis in non-small cell lung cancer and induces migration and tumor growth. J Thorac Oncol. 2011;6:1984–92.
22. Loewen G, Jayawickramarajah J, Zhuo Y, Shan B. Functions of lncRNA HOTAIR in lung cancer. J Hematol Oncol. 2014;7:90.
23. Dong J, Xu J, Wang X, Jin B. Influence of the interaction between long noncoding RNAs and hypoxia on tumorigenesis. Tumour Biol. 2016;37:1379–85.
24. Buffa FM, Harris AL, West CM, Miller CJ. Large meta-analysis of multiple cancers reveals a common, compact and highly prognostic hypoxia metagene. Br J Cancer. 2010;102:428–35.
25. Thai P, Statt S, Chen CH, Liang E, Campbell C, Wu R. Characterization of a novel long non-coding RNA, SCAL1, induced by cigarette smoke and elevated in lung cancer cell lines. Am J Respir Cell Mol Biol. 2013;49:204–11.
26. Volders PJ, Helsens K, Wang X, Menten B, Martens L, Gevaert K, et al. LNCipedia: a database for annotated human lncRNA transcript sequences and structures. Nucleic Acids Res. 2013;41:D246–D251.
27. Clark MB, Johnston RL, Inostroza-Ponta M, Fox AH, Fortini E, Moscato P, et al. Genome-wide analysis of long noncoding RNA stability. Genome Res. 2012;22:885–98.
28. Tani H, Mizutani R, Salam KA, Tano K, Ijiri K, Wakamatsu A, et al. Genome-wide determination of RNA stability reveals hundreds of short-lived noncoding transcripts in mammals. Genome Res. 2012;22:947–56.
29. Fitzpatrick SF, Tambuwala MM, Bruning U, Schaible B, Scholz CC, Byrne A, et al. An intact canonical NF-kappaB pathway is required for inflammatory gene expression in response to hypoxia. J Immunol. 2011;186:1091–6.
30. Rius J, Guma M, Schachtrup C, Akassoglou K, Zinkernagel AS, Nizet V, et al. NF-kappaB links innate immunity to the hypoxic response through transcriptional regulation of HIF-1alpha. Nature. 2008;453:807–11.
31. Toth RK, Warfel NA. Strange bedfellows: nuclear factor, erythroid 2-like 2 (Nrf2) and hypoxia-inducible factor 1 (HIF-1) in tumor hypoxia. Antioxidants (Basel). 2017;6:E27.
32. Burke JR, Pattoli MA, Gregor KR, Brassil PJ, MacMaster JF, McIntyre KW, et al. BMS-345541 is a highly selective inhibitor of I kappa B kinase that binds at an allosteric site of the enzyme and blocks NF-kappa B-dependent transcription in mice. J Biol Chem. 2003;278:1450–6.
33. Choi YM, Kim HK, Shim W, Anwar MA, Kwon JW, Kwon HK, et al. Mechanism of cisplatin-induced cytotoxicity is correlated to impaired metabolism due to mitochondrial ROS generation. PLoS ONE. 2015;10:e0135083.
34. Marullo R, Werner E, Degtyareva N, Moore B, Altavilla G, Ramalingam SS, et al. Cisplatin induces a mitochondrial-ROS

response that contributes to cytotoxicity depending on mitochondrial redox status and bioenergetic functions. PLoS ONE. 2013;8:e81162.
35. Shelton P, Jaiswal AK. The transcription factor NF-E2-related factor 2 (Nrf2): a protooncogene? FASEB J. 2013;27:414–23.
36. Singh A, Rangasamy T, Thimmulappa RK, Lee H, Osburn WO, Brigelius-Flohe R, et al. Glutathione peroxidase 2, the major cigarette smoke-inducible isoform of GPX in lungs, is regulated by Nrf2. Am J Respir Cell Mol Biol. 2006;35:639–50.
37. Liu X, Xavier C, Jann J, Wu H. Salvianolic acid B (Sal B) protects retinal pigment epithelial cells from oxidative stress-induced cell death by activating glutaredoxin 1 (Grx1). Int J Mol Sci. 2016;17:E1835.
38. Duong HQ, You KS, Oh S, Kwak SJ, Seong YS. Silencing of NRF2 reduces the expression of ALDH1A1 and ALDH3A1 and sensitizes to 5-FU in pancreatic cancer cells. Antioxidants (Basel). 2017;6:E52.
39. Woolbright BL, Choudhary D, Mikhalyuk A, Trammel C, Shanmugam S, Abbott E, et al. The role of pyruvate dehydrogenase kinase-4 (PDK4) in bladder cancer and chemoresistance. Mol Cancer Ther. 2018;17:2004–12.
40. Zhang Y, Zhang Y, Geng L, Yi H, Huo W, Talmon G, et al. Transforming growth factor beta mediates drug resistance by regulating the expression of pyruvate dehydrogenase kinase 4 in colorectal cancer. J Biol Chem. 2016;291:17405–16.
41. Wu X, Tudoran OM, Calin GA, Ivan M. The many faces of long noncoding RNAs in cancer. Antioxid Redox Signal. 2017;29:922–35.
42. Cabili MN, Trapnell C, Goff L, Koziol M, Tazon-Vega B, Regev A, et al. Integrative annotation of human large intergenic noncoding RNAs reveals global properties and specific subclasses. Genes Dev. 2011;25:1915–27.
43. Hangauer MJ, Vaughn IW, McManus MT. Pervasive transcription of the human genome produces thousands of previously unidentified long intergenic noncoding RNAs. PLoS Genet. 2013;9:e1003569.
44. Iyer MK, Niknafs YS, Malik R, Singhal U, Sahu A, Hosono Y, et al. The landscape of long noncoding RNAs in the human transcriptome. Nat Genet. 2015;47:199–208.
45. Fang S, Zhang L, Guo J, Niu Y, Wu Y, Li H, et al. NONCODEV5: a comprehensive annotation database for long noncoding RNAs. Nucleic Acids Res. 2018;46:D308–D314.
46. Harrow J, Frankish A, Gonzalez JM, Tapanari E, Diekhans M, Kokocinski F, et al. GENCODE: the reference human genome annotation for The ENCODE Project. Genome Res. 2012;22:1760–74.
47. Derrien T, Johnson R, Bussotti G, Tanzer A, Djebali S, Tilgner H, et al. The GENCODE v7 catalog of human long noncoding RNAs: analysis of their gene structure, evolution, and expression. Genome Res. 2012;22:1775–89.
48. Volders PJ, Verheggen K, Menschaert G, Vandepoele K, Martens L, Vandesompele J, et al. An update on LNCipedia: a database for annotated human lncRNA sequences. Nucleic Acids Res. 2015;43:4363–4.
49. Reuter S, Gupta SC, Chaturvedi MM, Aggarwal BB. Oxidative stress, inflammation, and cancer: how are they linked? Free Radic Biol Med. 2010;49:1603–16.
50. Tafani M, Sansone L, Limana F, Arcangeli T, De Santis E, Polese M, et al. The interplay of reactive oxygen species, hypoxia, inflammation, and sirtuins in cancer initiation and progression. Oxid Med Cell Longev. 2016;2016:3907147.
51. Eltzschig HK, Carmeliet P. Hypoxia and inflammation. N Engl J Med. 2011;364:656–65.
52. Gorlach A, Bonello S. The cross-talk between NF-kappaB and HIF-1: further evidence for a significant liaison. Biochem J. 2008;412:e17–19.
53. Oliver KM, Taylor CT, Cummins EP. Hypoxia. Regulation of NFkappaB signalling during inflammation: the role of hydroxylases. Arthritis Res Ther. 2009;11:215.
54. Patten DA, Lafleur VN, Robitaille GA, Chan DA, Giaccia AJ, Richard DE. Hypoxia-inducible factor-1 activation in nonhypoxic conditions: the essential role of mitochondrial-derived reactive oxygen species. Mol Biol Cell. 2010;21:3247–57.
55. Nakajima S, Kitamura M. Bidirectional regulation of NF-kappaB by reactive oxygen species: a role of unfolded protein response. Free Radic Biol Med. 2013;65:162–74.
56. Buelna-Chontal M, Zazueta C. Redox activation of Nrf2 & NF-kappaB: a double end sword? Cell Signal. 2013;25:2548–57.
57. Ashouri A, Sayin VI, Van den Eynden J, Singh SX, Papagiannakopoulos T, Larsson E. Pan-cancer transcriptomic analysis associates long non-coding RNAs with key mutational driver events. Nat Commun. 2016;7:13197.
58. White NM, Cabanski CR, Silva-Fisher JM, Dang HX, Govindan R, Maher CA. Transcriptome sequencing reveals altered long intergenic non-coding RNAs in lung cancer. Genome Biol. 2014;15:429.
59. Galluzzi L, Vitale I, Michels J, Brenner C, Szabadkai G, Harel-Bellan A, et al. Systems biology of cisplatin resistance: past, present and future. Cell Death Dis. 2014;**5**:e1257.
60. Zheng ZG, Xu H, Suo SS, Xu XL, Ni MW, Gu LH, et al. The essential role of H19 contributing to cisplatin resistance by regulating glutathione metabolism in high-grade serous ovarian cancer. Sci Rep. 2016;6:26093.
61. Sun Y, Jin SD, Zhu Q, Han L, Feng J, Lu XY, et al. Long noncoding RNA LUCAT1 is associated with poor prognosis in human non-small lung cancer and regulates cell proliferation via epigenetically repressing p21 and p57 expression. Oncotarget. 2017;8:28297–311.
62. Heery R, Finn SP, Cuffe S, Gray SG. Long non-coding RNAs: key regulators of epithelial-mesenchymal transition, tumour drug resistance and cancer stem cells. Cancers (Basel). 2017;9:38.
63. Hu Y, Zhu QN, Deng JL, Li ZX, Wang G, Zhu YS. Emerging role of long non-coding RNAs in cisplatin resistance. Onco Targets Ther. 2018;11:3185–94.
64. Yan W, Chen X. GPX2, a direct target ofp63, inhibits oxidative stress-induced apoptosis in a p53-dependent manner. J Biol Chem. 2006;281:7856–62.
65. Naiki T, Naiki-Ito A, Asamoto M, Kawai N, Tozawa K, Etani T, et al. GPX2 overexpression is involved in cell proliferation and prognosis of castration-resistant prostate cancer. Carcinogenesis. 2014;35:1962–7.
66. Liu X, Jann J, Xavier C, Wu H. Glutaredoxin 1 (Grx1) protects human retinal pigment epithelial cells from oxidative damage by preventing AKT glutathionylation. Invest Ophthalmol Vis Sci. 2015;56:2821–32.
67. Lassen N, Pappa A, Black WJ, Jester JV, Day BJ, Min E, et al. Antioxidant function of corneal ALDH3A1 in cultured stromal fibroblasts. Free Radic Biol Med. 2006;41:1459–69.
68. Muzio G, Maggiora M, Paiuzzi E, Oraldi M, Canuto RA. Aldehyde dehydrogenases and cell proliferation. Free Radic Biol Med. 2012;52:735–46.
69. Jang JH, Bruse S, Liu Y, Duffy V, Zhang C, Oyamada N, et al. Aldehyde dehydrogenase 3A1 protects airway epithelial cells from cigarette smoke-induced DNA damage and cytotoxicity. Free Radic Biol Med. 2014;68:80–6.
70. Leclerc D, Pham DN, Levesque N, Truongcao M, Foulkes WD, Sapienza C, et al. Oncogenic role of PDK4 in human colon cancer cells. Br J Cancer. 2017;116:930–6.
71. Khalil AM, Guttman M, Huarte M, Garber M, Raj A, Rivea Morales D, et al. Many human large intergenic noncoding RNAs associate with chromatin-modifying complexes and affect gene expression. Proc Natl Acad Sci USA. 2009;106:11667–72.

72. Davidovich C, Zheng L, Goodrich KJ, Cech TR. Promiscuous RNA binding by Polycomb repressive complex 2. Nat Struct Mol Biol. 2013;20:1250–7.
73. Blanco MR, Guttman M. Re-evaluating the foundations of lncRNA-Polycomb function. EMBO J. 2017;36:964–6.
74. Portoso M, Ragazzini R, Brencic Z, Moiani A, Michaud A, Vassilev I, et al. PRC2 is dispensable for HOTAIR-mediated transcriptional repression. EMBO J. 2017;36:981–94.
75. Engreitz JM, Haines JE, Perez EM, Munson G, Chen J, Kane M, et al. Local regulation of gene expression by lncRNA promoters, transcription and splicing. Nature. 2016;539:452–5.
76. Li W, Notani D, Rosenfeld MG. Enhancers as non-coding RNA transcription units: recent insights and future perspectives. Nat Rev Genet. 2016;17:207–23.
77. Lino Cardenas CL, Henaoui IS, Courcot E, Roderburg C, Cauffiez C, Aubert S, et al. miR-199a-5p Is upregulated during fibrogenic response to tissue injury and mediates TGFbeta-induced lung fibroblast activation by targeting caveolin-1. PLoS Genet. 2013;9:e1003291.
78. Lugthart S, Cheok MH, den Boer ML, Yang W, Holleman A, Cheng C, et al. Identification of genes associated with chemotherapy crossresistance and treatment response in childhood acute lymphoblastic leukemia. Cancer Cell. 2005;7:375–86.
79. Bertero T, Gastaldi C, Bourget-Ponzio I, Mari B, Meneguzzi G, Barbry P, et al. CDC25A targeting by miR-483-3p decreases CCND-CDK4/6 assembly and contributes to cell cycle arrest. Cell Death Differ. 2013;20:800–11.
80. Wang Y, Zhu W, Levy DE. Nuclear and cytoplasmic mRNA quantification by SYBR green based real-time RT-PCR. Methods. 2006;39:356–62.
81. Gastaldi C, Bertero T, Xu N, Bourget-Ponzio I, Lebrigand K, Fourre S, et al. miR-193b/365a cluster controls progression of epidermal squamous cell carcinoma. Carcinogenesis. 2014;35:1110–20.

Affiliations

Laura Moreno Leon[1,2] · Marine Gautier[1,2] · Richard Allan[1,2] · Marius Ilié[2,3,4] · Nicolas Nottet[1,2] · Nicolas Pons[1,2] · Agnes Paquet[1,2] · Kévin Lebrigand[1,2] · Marin Truchi[1,2] · Julien Fassy[1,2] · Virginie Magnone[1,2] · Garrett Kinnebrew[5] · Milan Radovich[5] · Meyling Hua-Chen Cheok[6] · Pascal Barbry[1,2] · Georges Vassaux[2,7] · Charles-Hugo Marquette[2,3,8] · Gilles Ponzio[1,2] · Mircea Ivan[9] · Nicolas Pottier[10] · Paul Hofman[2,3,4] · Bernard Mari[1,2] · Roger Rezzonico[2,7]

1 Université Côte d'Azur, CNRS UMR7275, IPMC, Valbonne, France

2 FHU-OncoAge, Nice, France

3 Université Côte d'Azur, CNRS, INSERM, IRCAN, Nice, France

4 Hospital-Related Biobank (BB-0033-00025), Pasteur Hospital, Nice, France

5 Department of Surgery, Medical and Molecular Genetics, Indiana University School of Medicine, Indianapolis, IN 46202, USA

6 INSERM UMR-S1172, Institute for Cancer Research of Lille, Factors of Leukemia Cell Persistence, Lille, Cedex, France

7 Université Côte d'Azur, INSERM, CNRS UMR7275, IPMC, Valbonne, France

8 Department of Pneumology, CHU-Nice, Nice, France

9 Department of Medicine and Department of Microbiology and Immunology, Indiana University School of Medicine, Indianapolis, IN 46202, USA

10 EA4483, Faculté de Médecine de Lille, Pole Recherche, Lille, France